ACS APPLIED BIO MATERIALS

www.acsabm.org Article

Effect of Alkyl Chain Length on the Photophysical, Photochemical, and Photobiological Properties of Ruthenium(II) Polypyridyl Complexes for Their Application as DNA-Targeting, Cellular-Imaging, and Light-Activated Therapeutic Agents

Sandra Estalayo-Adrián,* Salvador Blasco, Sandra A. Bright, Gavin J. McManus, Guillermo Orellana, D. Clive Williams, John M. Kelly, and Thorfinnur Gunnlaugsson*

Cite This: https://doi.org/10.1021/acsabm.1c00284 Read Online

ACCESS | Metrics & More | Article Recommendations | Supporting Information

ABSTRACT: A family of six Ru(II) polypyridyl complexes (**1**−**6**) which contain phenanthroline-based ligands functionalized with alkyl chains of different lengths (one methyl group, 10 and 21 carbon alkyl chains) and either 1,10-phenanthroline (phen) or 1,4,5,8-tetraazaphenanthrene (TAP) as ancillary ligands have been synthesized and characterized. The influence of the alkyl chain length on their photophysical and photochemical properties as well as in their photobiological applications has been elucidated by monitoring the changes in their MLCT-centered absorption and emission bands. The presence of one methyl group or 10 carbon alkyl chains does not seem to significantly affect the photophysical and photochemical properties of the resulting Ru(II) complexes when compared to the well-known $[Ru(phen)_3]^{2+}$ and $[Ru(TAP)_2phen]^{2+}$. However, an effect on their emission properties and in their ability to photosensitize singlet oxygen is observed for the Ru(II) complexes containing 21 carbon alkyl chains. The binding of these complexes to salmon testes DNA (stDNA) was investigated by observing the changes in the photophysical properties. Complexes **1**, **2**, **4**, and **5** all showed changes in their MLCT bands that could be analyzed using conventional fitting methods, such as the Bard equation. In contrast, complexes **3** and **6**, possessing long aliphatic chains, gave rise to nonclassic behavior. In addition to these analyses, both thermal denaturation and circular dichroism studies of **1**−**6** were carried out in the presence of stDNA which confirmed that these complexes bind to DNA. Confocal microscopy and viability studies in HeLa cervical cancer cells reveal an alkyl chain-length dependence on the cellular uptake and cytotoxicity of the resulting Ru(II) complexes due to an enhancement of their lipophilicity with increasing alkyl chain length. Thus, complexes containing 10 and 21 carbon alkyl chains are rapidly taken up into HeLa cells and, in particular, those with 21 carbon alkyl chains show a significant phototoxicity against the same cell line. Therefore, this study provides further insight into the possible modulation of the photophysical, photochemical, and photobiological properties of Ru(II) polypyridyl complexes by varying the length of the alkyl chains attached to the polypyridyl ligands coordinated to the Ru(II) center and the nature of the auxiliary groups, which we show has a significant effect on photophysical and biological properties.

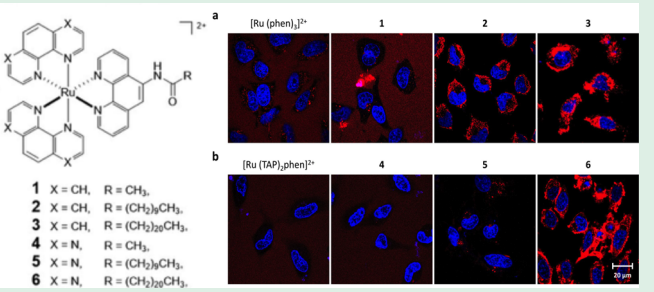

KEYWORDS: *ruthenium(II), polypyridyl complexes, luminescence, lipophilicity, anticancer, cellular imaging*

INTRODUCTION

Ruthenium(II) [Ru(II)] polypyridyl complexes have attracted much interest in the past number of decades for their interesting photophysical, photochemical, and redox properties.[1−3] Such complexes are characterized by their metal to ligand charge-transfer center (MLCT) absorption of light in the visible region (with λ_{max} from ca. 400 to 450 nm), luminescence in the red spectral range (with λ_{max} from ca. 600 to 650 nm), large Stokes shift, and relatively long luminescence lifetimes (typically from hundreds of nanoseconds to a few microseconds, due to ^{3}MLCT emission). These properties make Ru(II) polypyridyl complexes very attractive candidates for applications in photobiology as light-activated therapeutic agents and imaging probes, not only for targeting DNA but also in a cellular environment.[4−11] Therefore, the design of ruthenium-based systems with the ability to be internalized by the cells has become a crucial matter for such biological applications.

Received: March 8, 2021
Accepted: July 12, 2021

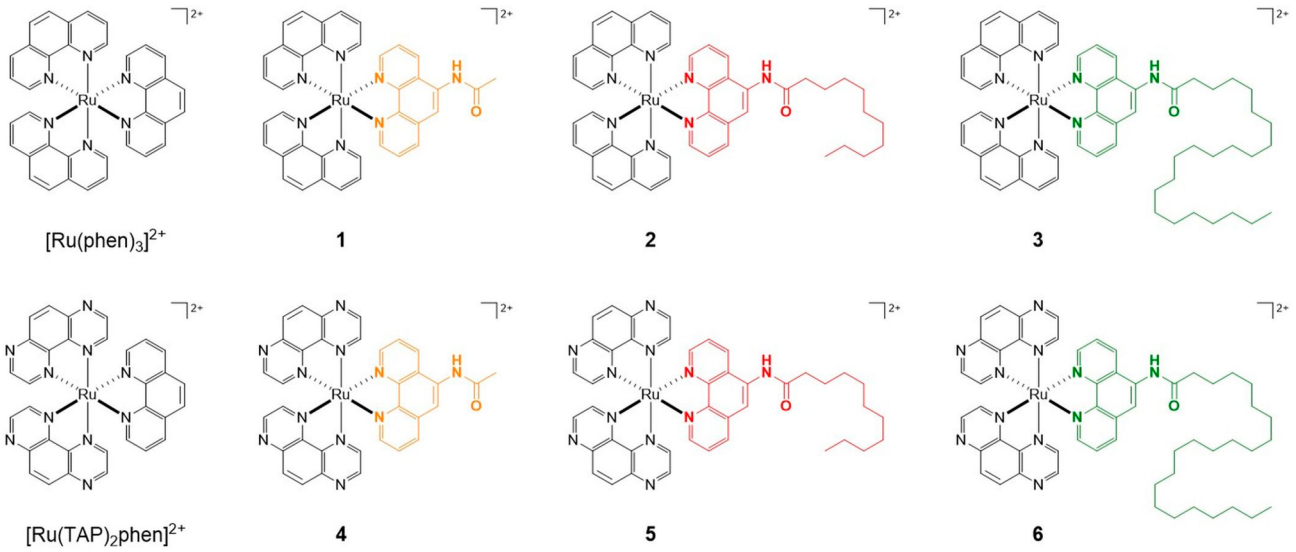

Figure 1. Chemical structures of the Ru(II) polypyridyl complexes $[Ru(phen)_3]^{2+}$ and $[Ru(TAP)_2phen]^{2+}$ and **1**−**6** studied in this work.

Factors such as molecule size, charge, and lipophilicity have been shown to play a key role in the cellular uptake mechanism and subcellular distribution of Ru(II) polypyridyl complexes, and thus, different strategies have been developed over the years with the aim of improving the cellular uptake of these complexes. For instance, these complexes have been conjugated to nanoparticles[12−17] and biomolecules such as peptides,[18−25] carbohydrates,[26−28] or lipids.[29−31] Another strategy consists of the coordination of lipophilic ligands to the Ru(II) center. In this context, the extension of the surface area of aromatic ligands such as the well-known [2,3-*h*]dipyrido[3,2-*a*:2′,3′-*c*]phenazine (dppz) has been shown to confer lipophilicity to the resulting Ru(II) complex and enhance their cellular uptake.[32−34] Other lipophilic ligands include 7-diphenyl-1,10-phenanthroline (dip) or alkyl chain-based derivatives which have been shown to increase the intracellular internalization of the complexes when compared to their more hydrophilic analogues.[35,36]

The incorporation of lipophilic tails to the hydrophilic ruthenium-based core also provides the resulting molecule with an amphiphilic character and a general structural resemblance to biological lipids, thus facilitating their insertion into the lipid bilayer that constitutes the cell membrane.[37] Lipid mimetic luminescent Ru(II) polypyridyl complexes have been developed for their potential use in labeling liposomes and phospholipids membranes.[38−40] Furthermore, the presence of hydrophobic alkyl chains has been shown to have an effect not only on the lipophilicity of the Ru(II) complexes but also on their ability to form self-assembly supramolecular structures in aqueous solution acting as metallosurfactants. They have been extensively used in recent years in imaging and drug delivery applications.[41−43] The presence of metals in the headgroup of these amphiphilic structures confers them with advantageous properties.[44] In this context, Ru(II)-based metallosurfactants have shown great potential in several biological applications such as in the imaging of physiological hypoxia, phospholipid membranes labeling, gene therapy, or anticancer agents.[40,45−47]

The addition of new functionalities to the ligands coordinated to the Ru(II) center can have a dramatic effect on the photophysical and photochemical properties of the resulting Ru(II) complexes and as such influence their photobiological behavior when evaluated in a cellular environment.[1] With this in mind, we report herein, the synthesis and characterization of a family of Ru(II) polypyridyl complexes (**1**−**6**) containing different lengths of alkylamide functionalized phenanthroline ligands (**7**−**9**, one methyl group, 10 and 21 carbon alkyl chains, respectively) and either 1,10-phenanthroline (phen) or 1,4,5,8-tetraazaphenanthrene (TAP) as ancillary ligands (Figure 1). The effect of the alkyl chain length on their photophysical and photochemical properties and their ability to bind to DNA as well as the impact on their cellular uptake and application as light-activated therapeutic agents is investigated. No significant effect on the photophysical properties of complexes containing one methyl group or 10 carbon alkyl chains was observed when compared to the well-known parent complexes $[Ru(phen)_3]^{2+}$ and $[Ru(TAP)_2phen]^{2+}$. However, the extension of the alkyl chain to 21 carbons affects the emission properties of the resulting Ru(II) complexes as well as their ability to produce singlet oxygen. Furthermore, the enhancement of the lipophilicity with the increasing alkyl chain length results in an improvement of the cellular uptake of the complexes and, as such, of their phototoxicity against HeLa cervical cancer cells, suggesting a possible modulation of the toxicity when designing Ru(II) polypyridyl complex-based light-activated therapeutic agents by varying the alkyl chain length. In this contribution we give a full account of our work involving **1**−**6**. Part of this research, dealing with the self-assembly formation of **3** and **6**, respectively, and some photophysical and biological profiling, was recently communicated.[21]

RESULTS AND DISCUSSION

Synthesis of Ligands and Complexes. The synthesis of the Ru(II) polypyridyl complexes **1**−**6** was achieved according to a procedure previously used in our laboratory (Scheme 1).[12,15,33,34,48] First, ligand **7** was prepared following a method described in the literature based on the amide coupling reaction between 5-amino-1,10-phenanthroline (**10**) and acetic anhydride (**11**) in MeCN.[49] Ligand **8** was synthesized using the same synthetic strategy reported by us in a previous work for ligand **9**, which consists of the amide coupling reaction

https://doi.org/10.1021/acsabm.1c00284
ACS Appl. Bio Mater. XXXX, XXX, XXX−XXX

Scheme 1. Synthesis of the Ru(II) Polypyridyl Complexes 1−6[a]

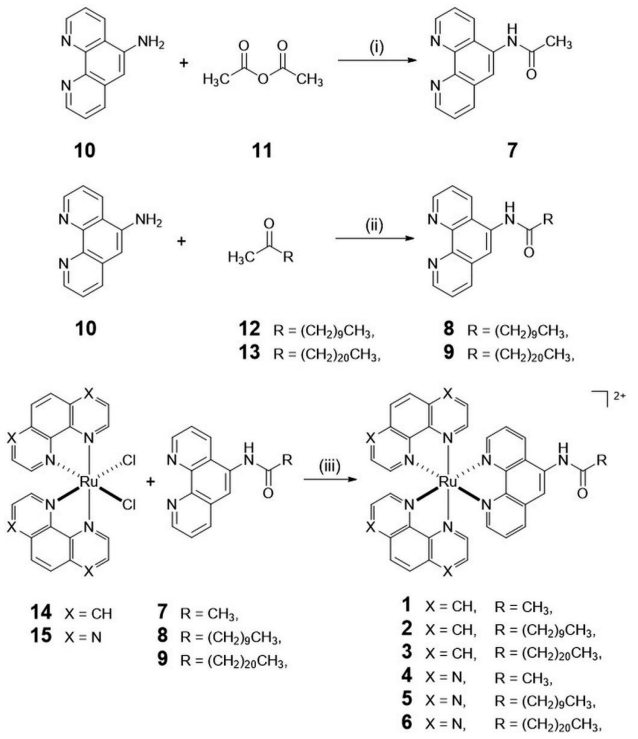

[a]Conditions: (i) CH_3CN, r.t., 2 days; (ii) EDC, DMAP, CH_2Cl_2, r.t., 2 days; (iii) EtOH/H_2O (1:1), microwave reaction, 140 °C, 40 min (**1**−**3**) or 10 min (**4**−**6**).

between **10** and undecanoic acid (**12**) in the case of **8**, or docosanoic acid (**13**) in the case of **9**, using *N*-ethyl-*N*′-(3-(dimethylamino)propyl)carbodiimide hydrochloride (EDC) in the presence of 4-(dimethylamino)pyridine (DMAP) in dry DCM.[48] Ligands **7**−**9** were obtained as beige solids in 62, 57, and 95% yields, respectively. Ru(II) complexes **1**−**6** were subsequently prepared by microwave-assisted reaction using the appropriate Ru(II) *cis*-bispolypyridyl dichloride precursor complex (**14** or **15**) and the corresponding *N*-1,10-phenanthrolin-5-yl-alkylamide ligand (**7**−**9**) in a H_2O/EtOH (1:1) mixture at 140 °C for 40 (**1**−**3**) or 10 min (**4**−**6**). The chloride salts of **1**−**6** were obtained as red solids in 60, 60, 50, 52, 43, and 42% yields, respectively, after purification by column chromatography on neutral alumina using MeCN/H_2O (10:0 to 9:1) as eluent. Ligands **7**−**9** and complexes **1**−**6** were fully characterized by conventional methods, including the use of ^{1}H NMR and ^{13}C NMR spectroscopies, elemental analysis, HRMS, melting point analysis, and IR spectroscopy (Figures S1−S22, Supporting Information).

Photophysical Characterization. In order to gain a better insight into the impact the alkyl chain length has on the absorption and emission properties of the synthesized Ru(II) complexes, the photophysical properties of **1**, **2**, **4**, and **5** were investigated in 10 mM sodium phosphate-buffered aqueous solution at pH 7.4 and 298 K, and the results were compared to those previously reported by us for **3** and **6**, and for the well-known parent complexes $[Ru(phen)_3]^{2+}$ and $[Ru(TAP)_2phen]^{2+}$, respectively.[48]

Complexes containing phen as ancillary ligands (**1**−**3**) showed absorption spectra similar to that recorded for $[Ru(phen)_3]^{2+}$ (Figure 2a and Table 1) with the $\pi-\pi^*$ intraligand transitions of the phen ligand localized at ca. 220 and 260 nm, while the broad band center at ca. 450 nm was attributed to the characteristic MLCT transition in the metallic complexes.[50] Likewise, absorption maxima similar to those recorded for $[Ru(TAP)_2phen]^{2+}$ were observed for the complexes containing TAP as ancillary ligands (**4**−**6**) (Figure 2b and Table 1).[51] Thus, intense bands at ca. 230 and 270 nm are attributed to $\pi-\pi^*$ intraligand transitions in the TAP ligand, and the broad band cantered at ca. 415 nm corresponds to the MLCT transition of the Ru(II) center.

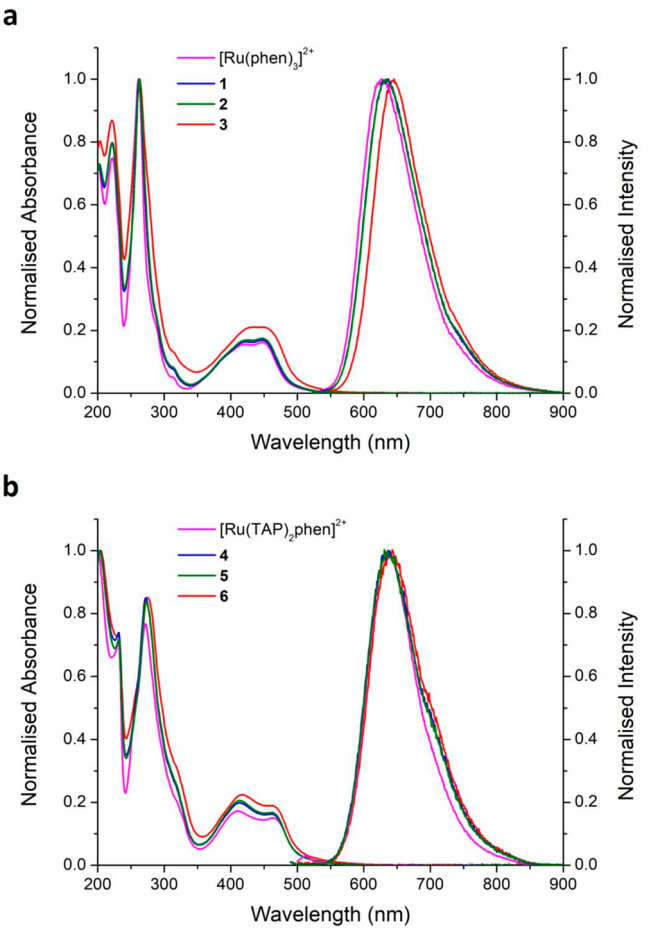

Figure 2. UV−vis absorption and emission spectra of (a) $[Ru(phen)_3]^{2+}$ and **1**−**3** and (b) $[Ru(TAP)_2phen]^{2+}$ and **4**−**6** in aerated 10 mM sodium phosphate-buffered aqueous solution at pH 7.4 and 298 K (λ_{exc} = 440 nm ($[Ru(phen)_3]^{2+}$ and **1**−**3**), 436 nm ($[Ru(TAP)_2phen]^{2+}$), 413 nm (**4** and **5**), or 418 nm (**6**)).

Excitation into the MLCT bands of each complex resulted in broad emission bands centered at 606 and 603 nm for **1** and **2**, respectively (Figure 2a). These values are very close to the emission maximum observed for $[Ru(phen)_3]^{2+}$.[50] However, as we showed in our previous work,[48] a slightly red-shifted emission band at 614 nm was observed for **3** when compared to $[Ru(phen)_3]^{2+}$. Similarly, the emission spectra of **4** and **5** exhibited broad bands centered at 636 nm (Figure 2b), while the emission maximum at 643 nm of **6** was found to be slightly red-shifted compared to that observed for $[Ru(TAP)_2phen]^{2+}$.[51] The excitation spectra recorded for these complexes were found to be identical to their absorption spectra (Figure S23, Supporting Information).

Luminescence quantum yields (Φ_{em}) were determined in aerated 10 mM sodium phosphate-buffered aqueous solution

https://doi.org/10.1021/acsabm.1c00284
ACS Appl. Bio Mater. XXXX, XXX, XXX−XXX

Table 1. Absorption and Emission Properties of 1, 2, 4, and 5 in 10 mM Sodium Phosphate-Buffered Aqueous Solution at pH 7.4 and 298 K[a]

	λ_{max} (nm) (ε, 10^4 M^{-1} cm^{-1})[b]		emission				
complex	$\pi-\pi^*$ IL	$\pi-\pi^*$ MLCT	λ_{max}^{em} (nm)	Φ_{em}[c] (air)	τ_{em} (ns)[d] (air)	τ_{em} (ns)[d] (N_2)	$P_{O_2}^T$ (air-satd)
$[Ru(phen)_3]^{2+}$	224, 262[e]	447 (1.90)[e]	604[e]	0.050	480[e]	990[e]	0.52
1	221 (7.83), 262 (9.88)	447 (1.67)	606	0.057	644	1300	0.50
2	222 (7.91), 262 (10.0)	448 (1.76)	603	0.060	650	1270	0.49
3[f]	222 (6.60), 263 (7.60)	451 (1.60)	614	0.070	1085[g]	1354[g]	0.20
$[Ru(TAP)_2phen]^{2+}$	230 (6.12), 272 (6.93)[h]	410 (1.65)[h]	645[h]	0.029	690[h]	835[h]	0.17
4	232 (5.78), 272 (6.64)	414 (1.56)	636	0.033	538	636	0.15
5	232 (6.07), 273 (7.08)	413 (1.74)	636	0.034	570	674	0.15
6[f]	230 (5.18), 274 (6.06)	418 (1.59)	643	0.017	587[g]	696[g]	0.16

[a]Complexes $[Ru(phen)_3]^{2+}$, **3**, $[Ru(TAP)_2phen]^{2+}$ and **6** are included for comparison.[48,50,51]. [b]λ_{max}, absorbance. Estimated uncertainty ±1%. [c]Air-saturated aqueous solution of $[Ru(bpy)_3]Cl_2$ as reference (Φ_{em} = 0.040).[58] Estimated uncertainty ±5%. [d]If not otherwise indicated, the luminescence decays are monoexponential. Estimated uncertainty ±10%. [e]Herman et al.[50] The reported values are in aqueous solution. [f]Estalayo-Adrián et al.[48] [g]The luminescence decays are biexponential; reported data correspond to the pre-exponential weighted mean lifetimes (τ_M) and were calculated according to $\tau_M = \sum(a_i\tau_i)/\sum a_i$.[56] [h]Ortmans et al.[51] The reported values are in aqueous solution.

at pH 7.4 and revealed an influence of the alkyl chain length (Table 1). Complexes **1**−**3** showed Φ_{em} of 0.057, 0.060, and 0.070, respectively, while Φ_{em} of 0.033, 0.034, and 0.017 were observed for the TAP analogous complexes **4**−**6**, respectively.[58] The values observed for **1** and **2** and for **4** and **5** are similar to those determined for $[Ru(phen)_3]^{2+}$ and $[Ru(TAP)_2phen]^{2+}$, respectively. However, in line with what we showed in our previous work,[21] **3** exhibits a slightly higher Φ_{em} when compared to those displayed by $[Ru(phen)_3]^{2+}$, **1** and **2**. In contrast, **6** shows the opposite effect and a lower Φ_{em} was observed than those exhibited for $[Ru(TAP)_2phen]^{2+}$, **4**, and **5**.

Complexes **1** and **2** showed luminescence lifetimes (τ_{em}) of 644 and 650 ns, respectively, in aerated 10 mM sodium phosphate-buffered aqueous solution at pH 7.4. Solution deoxygenation resulted in a significant increase in the excited-state lifetimes with values of 1300 and 1270 ns for **1** and **2**, respectively. Similarly, in aerated solution τ_{em} of 538 and 570 ns were observed for the TAP analogue complexes **4** and **5**, respectively. Only slightly longer τ_{em} of 636 and 674 ns, respectively, were observed when solutions containing **4** and **5** were deoxygenated. These results demonstrate that the luminescence of the excited state of TAP complexes is less affected by the presence of dissolved oxygen than that of complexes containing phen as ancillary ligands. This is in agreement with previous work reported in the literature[23,52−54] and was further corroborated through calculation of the values of the proportion of triplet excited states quenched by O_2 ($P_{O_2}^T$) for both phen and TAP complexes.[55] Hence, phen derivatives display $P_{O_2}^T$ values of ca. 0.50, while the TAP analogues exhibit smaller values of ca. 0.15, showing a larger efficiency of quenching of the excited states of the phen complexes by oxygen than those of the TAP complexes. Furthermore, whereas emission decay curves for **1**, **2**, **4**, and **5** could be fitted to a monoexponential function, luminescence lifetime data for **3** and **6**, as reported in our previous work,[21] required biexponential fits, and as such the values shown here correspond to the pre-exponential weighted mean lifetimes (τ_M).[56] Since these compounds contain long alkyl chains, the presence of different emitting species may be due either to the formation of aggregates or possibly to the long alkyl chain interacting with the hydrophobic phen ligand. The phen complex **3** showed τ_M values of 1085 and 1354 ns in aerated and deoxygenated aqueous solutions, respectively, which are longer than those reported for **1** and **2**. This can be attributed to the excited state of **3**, both being less susceptible to nonradiative deactivation and also being protected from oxygen quenching. This gives rise to a lower $P_{O_2}^T$ value for **3** when compared to **1**. Similar behavior has previously been reported in the literature for related Ru(II) complexes.[57]

In contrast to what is found for the phen complexes, τ_M values of 587 and 696 ns were observed for the TAP analogue **6** in both aerated and deoxygenated aqueous solutions, respectively, similar to the values measured for **4** and **5**. The $P_{O_2}^T$ value displayed by **6** was also comparable to those determined for **4** and **5**. These measurements show that overall the long alkyl chain does not have a significant effect on either the nonradiative decay or the oxygen quenching of the excited state of **6**.

To further investigate the effect of the long alkyl chain on the photophysical behavior of **3** and **6**, and based on our previous work where we demonstrated the ability of these complexes to self-aggregate in solution into micellar species (critical micelle concentration (cmc) of 114 and 113 μM were determined for **3** and **6**, respectively),[48] luminescence lifetimes of aerated aqueous solutions of **3** and **6** at different concentrations (below and above their cmc) were measured (Figure 3). As expected, biexponential fits were needed for the luminescence decay kinetics at all concentrations and thus τ_M were calculated (Tables S1 and S2, Supporting Information). Interestingly, the increase of the complex concentration had an opposite effect on the τ_M values of both **3** and **6**. Thus, while the phen complex showed larger τ_M values when the concentration of the complex was increased, the τ_M values of the TAP analogue were shorter at larger complex concentrations. The reasons for this (whether due to changes to the nonradiative decay rate, protection from oxygen quenching, or possible self-quenching upon aggregation) will require further detailed study beyond the scope of the current publication.

Singlet Oxygen Photosensitization. Singlet oxygen ($^1O_2$) photosensitization is one of the possible modes of action (Type II mechanism) of the molecules used in photodynamic therapy (PDT).[7] Therefore, quantum yields of $^1O_2$ production (Φ_Δ) of **1**, **2**, **4**, and **5** were determined in O_2-saturated D_2O by direct measurement of $^1O_2$ phosphorescence at 1265 nm (following excitation of the complex at 532 nm). These may be compared to those previously determined for

https://doi.org/10.1021/acsabm.1c00284
ACS Appl. Bio Mater. XXXX, XXX, XXX−XXX

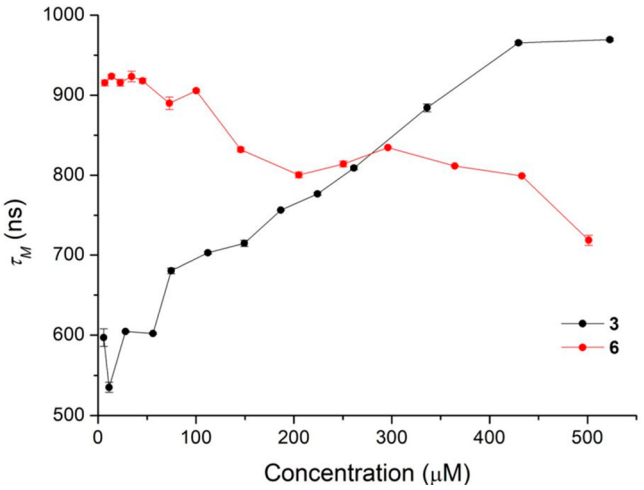

Figure 3. Evolution of the pre-exponential weighted mean lifetime (τ_M) of aerated aqueous solutions of **3** and **6** at different concentrations, at 298 K.

$[Ru(phen)_3]^{2+}$, **3**, $[Ru(TAP)_2phen]^{2+}$, and **6** (Table 2 and Figure S24, Supporting Information) and show how the Φ_Δ of these complexes are affected by the presence of different length alkyl chains.[48,59] It should be noted that D_2O was used as solvent instead of regular H_2O due to the much shorter $^1O_2$ lifetime in H_2O compared to its deuterated analogue. However, knowing the Φ_Δ values in H_2O and in aerated solution is more relevant when extrapolating to biological systems. Thus, the Φ_Δ values obtained in O_2-saturated D_2O were converted into those in air-saturated H_2O (see Experimental Section, Tables 2 and S3, Supporting Information).

Production of $^1O_2$ was shown to be dependent on the nature of the ancillary ligands (phen or TAP) and on the alkyl chain length. Complexes $[Ru(TAP)_2phen]^{2+}$ and **4**–**6** containing TAP as ancillary ligands displayed higher Φ_Δ values than their phen analogues in O_2-saturated D_2O. This behavior can be explained by the fact that the excited-state reduction potentials of the TAP complexes are significantly higher than those of the phen analogues, resulting in a considerable slowing of the superoxide competing route that requires photoinduced electron transfer (PET) from the Ru(II) complex to O_2.[55,60] This is supported by the values of the fraction of triplet excited states quenched by O_2 yielding $^1O_2$ (f_Δ^T) determined for each complex (Table 2). Thus, phen-containing complexes $[Ru(phen)_3]^{2+}$, **1**, and **2** showed f_Δ^T values of 0.46, 0.60, and 0.51 vs 1.00, 0.93, and 0.79 observed for their TAP analogues $[Ru(TAP)_2phen]^{2+}$, **4**, and **5**.

In contrast, when Φ_Δ values were converted from O_2-saturated D_2O to air-saturated H_2O conditions, $[Ru(phen)_3]^{2+}$ and **1**–**3** containing phen as ancillary ligands displayed higher Φ_Δ values than their TAP analogues $[Ru(TAP)_2phen]^{2+}$ and **4**–**6**. This is due to a lower efficiency of quenching of the excited states of TAP complexes by oxygen in H_2O when compared with the phen complexes. The calculated values of the proportion of triplet excited states quenched by O_2 ($P_{O_2}^T$) in air-saturated H_2O confirmed this fact with $P_{O_2}^T$ values of ca. 0.50 and 0.20 observed for phen and TAP complexes, respectively, with the exceptions of **3** and **6** (Table 2).[55]

These complexes containing the 21 carbon alkyl chain show much lower Φ_Δ values, which may be attributed to them being in a micellar state, as the direct measurement of the $^1O_2$ phosphorescence requires a high concentration of photosensitizer (ca. 300 μM). This demonstrates that the aggregation state can have an effect on the interaction between the Ru-centered MLCT excited state and molecular oxygen. Therefore, the ability of **3** and **6** to produce $^1O_2$ is concentration dependent, depending on whether they are free in solution or forming micelles.

The effective production of $^1O_2$ by **1**, **2**, **4**, and **5** was also demonstrated by using the water-soluble $^1O_2$ chemical probe, 9,10-anthracenediylbis(methylene)dimalonic acid (ABDA).[61] This molecule is known to be photo-oxidized by $^1O_2$, resulting in a non-emissive endoperoxide product. Thus, the changes in the emission spectra of ABDA in air-saturated H_2O and in the presence of **1**, **2**, **4**, and **5** upon different irradiation times (470 nm LED source) were monitored (Figure S25, Supporting Information) and compared to those observed for $[Ru(phen)_3]^{2+}$, **3**, $[Ru(TAP)_2phen]^{2+}$, and **6** in our previous work.[21] A decrease in the emission intensity of ABDA at 405 nm was observed as the irradiation time increased, consistent with the generation of $^1O_2$ by all of the Ru(II) complexes tested.[62]

Interestingly, the rate of disappearance of the ABDA fluorescence was affected by the presence of long alkyl chains

Table 2. Quantum Yields of Singlet Oxygen Production (Φ_Δ) of 1, 2, 4, and 5 ($A_{532} \approx 0.40$) Determined by Time-Resolved Near-Infrared Phosphorescence (λ_{exc} = 532 nm)[a]

	direct detection of $^1O_2$ (time-resolved NIR phosphorescence)					indirect detection of $^1O_2$ ($^1O_2$ probe ABDA)	
complex	Φ_Δ (O_2-satd D_2O)[b]	Φ_Δ (air-satd H_2O)[c]	$P_{O_2}^T$ (O_2-satd D_2O)[d]	$P_{O_2}^T$ (air-satd H_2O)[d]	f_Δ^T (O_2-satd D_2O)[d]	Φ_Δ (air-satd H_2O)[e]	% photobleaching (405 nm, 10 s irradiation)
$[Ru(phen)_3]^{2+}$	0.39	0.21	0.84	0.46	0.46	0.22	5[f]
1	0.52	0.31	0.86	0.50	0.60	0.23	5
2	0.44	0.24	0.87	0.48	0.51	0.23	4
3	0.18[f]	0.03[f]	0.50	0.08	0.36		83[f]
$[Ru(TAP)_2phen]^{2+}$	0.72	0.14	0.72	0.14	1.00		19[f]
4	0.69	0.18	0.74	0.19	0.93		22
5	0.59	0.16	0.75	0.20	0.79		18
6	0.14[f]	0.01[f]	0.50	0.08	0.28		73[f]

[a]Complexes $[Ru(phen)_3]^{2+}$, **3**, $[Ru(TAP)_2phen]^{2+}$, and **6** are included for comparison.[48]. [b]O_2-saturated D_2O solution of $[Ru(phen)_3]Cl_2$ as reference (Φ_Δ = 0.39).[59] Estimated errors ±5%. [c]Calculated from the values obtained in O_2-saturated D_2O and knowing the emission lifetimes of the complexes in O_2- and Ar-saturated D_2O, and air- and Ar-saturated H_2O (see Experimental Section and Table S3, Supporting Information).[59] [d]Calculated according to $P_{O_2}^T = 1 - \tau/\tau_0$.[59] [e]Air-saturated H_2O solution of $[Ru(bpy)_3]Cl_2$ as reference (Φ_Δ = 0.18).[67] [f]Estalayo-Adrián et al.[48]

https://doi.org/10.1021/acsabm.1c00284
ACS Appl. Bio Mater. XXXX, XXX, XXX−XXX

(Figure 4 and Table 2). Thus, the intensity of the ABDA emission band at 405 nm was shown to decrease by ca. 5%

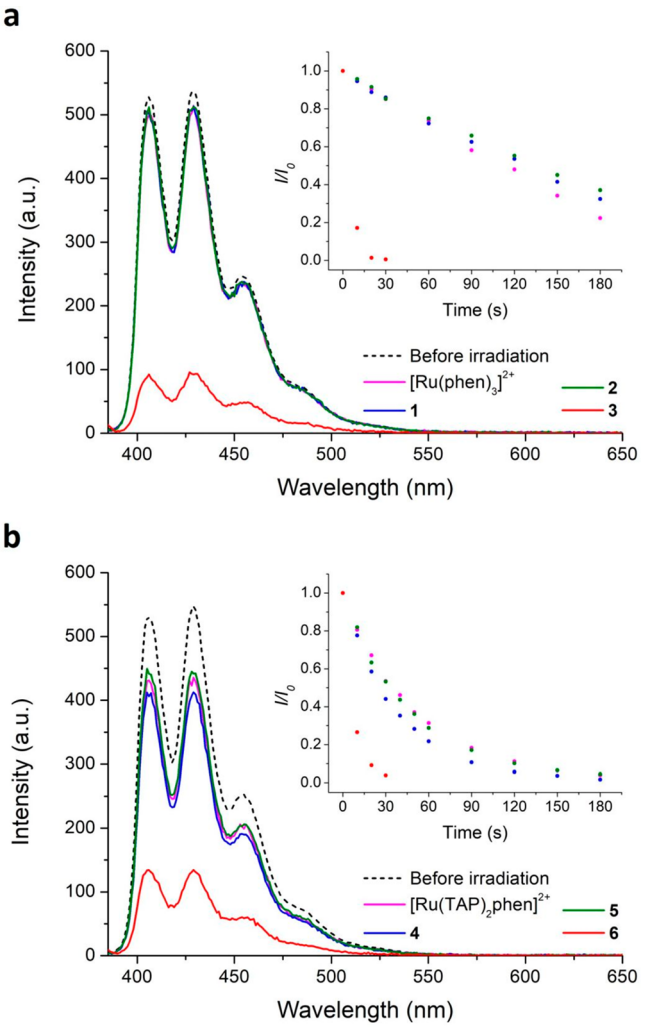

Figure 4. Emission spectra of ABDA (λ_{exc} = 380 nm) in the presence of (a) $[Ru(phen)_3]^{2+}$ and **1**–**3** and (b) $[Ru(TAP)_2phen]^{2+}$ and **4**–**6** ($A_{470} \approx 0.01$) in air-saturated aqueous solution before irradiation and after 10 s irradiation using a 470 nm LED source at 298 K. Inset: Rate of decay of ABDA emission band at 405 nm photosensitized by the corresponding Ru(II) complex.

after 10 s irradiation in the presence of the phen complexes $[Ru(phen)_3]^{2+}$, **1**, and **2** and by ca. 20% when the TAP analogues $[Ru(TAP)_2phen]^{2+}$, **4**, and **5** were used as photosensitizers. These Φ_Δ values determined for $[Ru(phen)_3]^{2+}$, **1**, and **2** were found to be similar to those obtained by time-resolved NIR phosphorescence from $^1O_2$ in air-saturated H_2O (Table 2).

In contrast to what was found with the other complexes, decreases of 83% and 73% of the ABDA emission band were observed in the presence of those containing the 21 carbon alkyl chain, **3** and **6**. The reason for the fast decrease of the ABDA emission band with the irradiation time in the presence of these complexes is unclear and will require further study, although a hydrophobic interaction between the $^1O_2$ chemical probe and the alkyl chain of **3** and **6** should be considered. For this reason, the Φ_Δ value of **3** could not be quantified due to the fast consumption of the ABDA under irradiation in the presence of this complex. In addition, the consumption of the $^1O_2$ chemical probe was found to decrease exponentially over time in the presence of the TAP derivatives $[Ru(TAP)_2phen]^{2+}$ and **4**–**6**, in contrast to the linear decrease observed for the phen complexes $[Ru(phen)_3]^{2+}$, **1**, and **2** (Figure 4). As was anticipated in our previous work, this behavior can be explained by the remarkably photo-oxidant character of the excited state of Ru(II) complexes containing at least two TAP ligands providing them with the ability to directly photo-oxidize the ABDA.[48,63,64] Thus, the coexistence of two competitive processes, that is oxidation of the chemical probe by $^1O_2$ production and/or by the TAP complex, can be presumed with the latter dominating. Oxidation of anthracene derivatives by electron-transfer photosensitizers has been previously described.[65] This hypothesis is supported by the redox potentials reported in the literature for $[Ru(TAP)_2phen]^{2+}$ (E_{red}^* = +1.15 V/SCE)[51] and 9,10-dimethylanthracene (E_{ox} = +1.05 V/SCE).[65,66] From these values it can be concluded that direct photo-oxidation of 9,10-dimethylanthracene by $[Ru(TAP)_2phen]^{2+}$ is slightly thermodynamically favorable (ΔG^0 = −0.10). These observations suggest that anthracene-based $^1O_2$ probes are not suitable for photosensitizers with a high photo-oxidant excited state such as TAP-containing complexes, and as such, Φ_Δ values for $[Ru(TAP)_2phen]^{2+}$ and **4**–**6** could not be determined through this method.

DNA Binding Studies. Having investigated the photophysical properties of **1**–**6** in solution, we next investigated their ability to bind to DNA. Ru(II) polypyridyl complexes, of the nature presented herein, are known DNA binders. This is due to their cationic nature, as well as the extended polypyridyl ligands which can partially intercalate both between the DNA bases or though groove binding.[3,12,17] The added complexity of our design, i.e., the presence of alkyl chains of different lengths, made us curious to investigate if these and, in particular, **3** and **6**, would behave as "classic" examples of Ru(II) complexes such as $[Ru(phen)_3]^{2+}$ and $[Ru(TAP)_2phen]^{2+}$ upon interacting with DNA or if their self-assembly nature would overwrite such classic binding behavior, which we might expect to see for **1**, **2**, **4**, and **5**.

The binding interactions of **1**–**6** were investigated using salmon testes DNA (stDNA) by observing the changes in their MLCT absorption and emission properties upon gradual addition of aliquots of stDNA to a 10 mM sodium phosphate-buffered aqueous solution at pH 7.4 containing the corresponding Ru(II) complex. Changes in the MLCT absorption band as well as in the emission intensity were monitored spectroscopically until no significant changes were detected at increasing stDNA concentrations. All titrations were repeated at least three times to ensure reproducibility. Complexes **1** and **2** exhibited a 14% and 33% decrease in the absorption of the MLCT band at 447 and 448 nm, respectively, upon addition of stDNA (Figure 5a,c). However, a more complex behavior was observed for **3**, where an initial decrease in the absorption of the MLCT band at 451 nm was observed after the addition of 0.5 equiv of stDNA, followed by a strong increase in this absorption band upon the addition of stDNA up to 2.2 equiv (Figure 5e); these overall changes ended in a slight decrease until the absorption plateau was reached. Concomitantly, a red shift of ca. 15 nm in the MLCT band was observed. Hence, while **1** and **2** give rise to more "typical" binding interactions with DNA, the changes observed for **3** seem to indicate that the long chain modulates these interactions. The changes in the MLCT emission were

https://doi.org/10.1021/acsabm.1c00284
ACS Appl. Bio Mater. XXXX, XXX, XXX−XXX

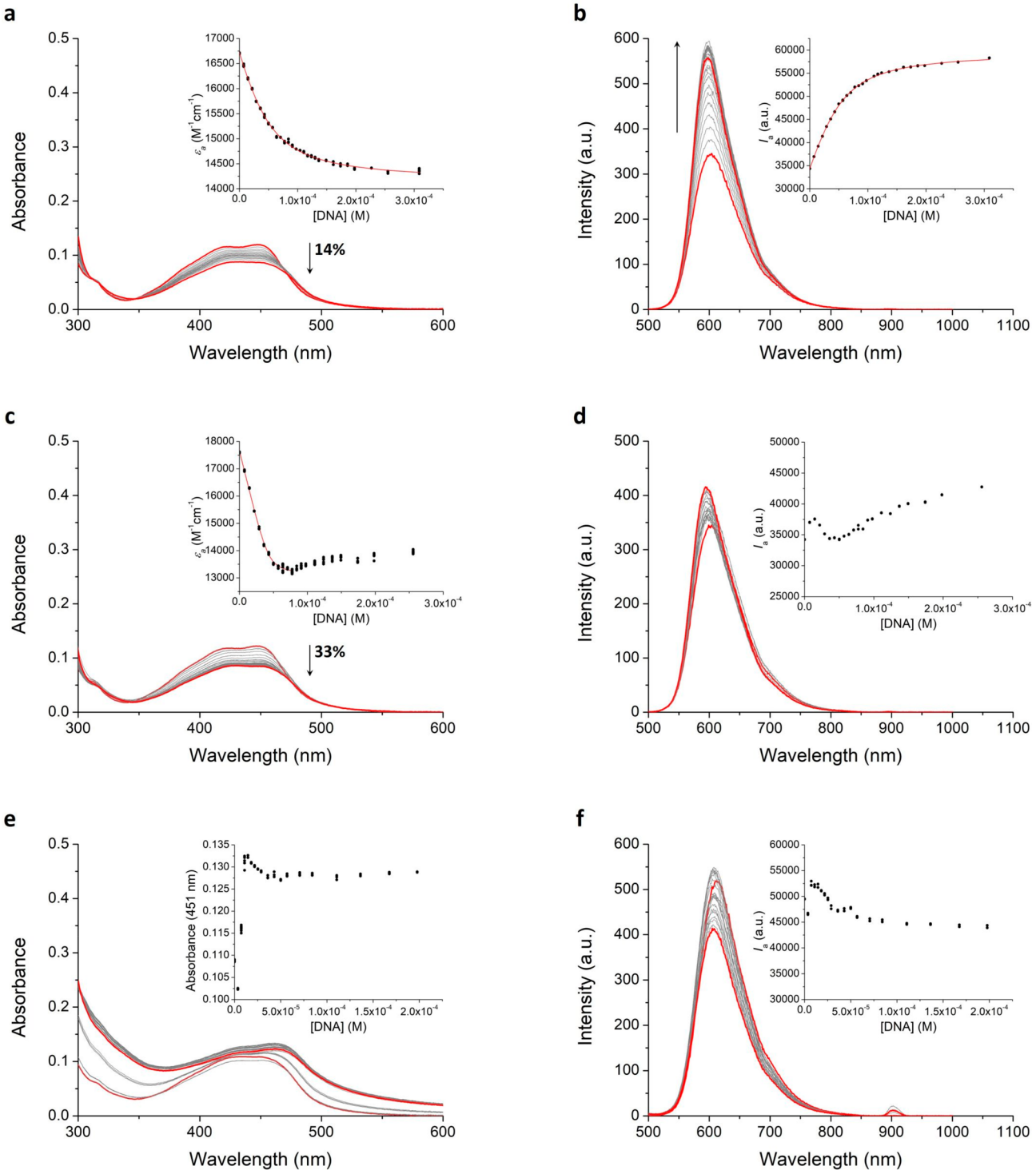

Figure 5. Changes in the UV−vis absorption and emission spectra of (a, b) **1** (7.16 μM, λ_{exc} = 447 nm), (c, d) **2** (6.94 μM, λ_{exc} = 448 nm), and (e, f) **3** (6.79 μM, λ_{exc} = 451 nm) with increasing concentration of stDNA (0−309, 0−256, and 0−198 μM, respectively) in 10 mM sodium phosphate-buffered aqueous solution at pH 7.4. Inset: Plot of ε_a (M^{-1} cm^{-1}) or I_a (a.u.) vs [DNA] (M, bases) using data from absorbance at (a) 447, (c) 448, and (e) 451 nm or integrated MLCT emission intensity (b, d, f) and the best fit of the data, when possible, using a modification of the Bard equation.

concomitantly recorded upon each addition of stDNA, where it was observed that **1** displayed an enhancement in the MLCT emission intensity centered at 603 nm, together with a blue shift of ca. 6 nm over the course of the titration (Figure 5b). A triphasic behavior was, however, exhibited by **2** for which the emission intensity at 604 nm enhanced upon the addition of 2.1 equiv of stDNA, followed by a decrease up to 7.4 equiv of stDNA, and by an increase again until emission intensity did not experience significant changes upon further increasing in the stDNA concentration (Figure 5d). Complex **3** also showed a triphasic behavior starting with a decrease in the emission intensity, centered at 612 nm, after the addition of 0.5 equiv of

https://doi.org/10.1021/acsabm.1c00284
ACS Appl. Bio Mater. XXXX, XXX, XXX−XXX

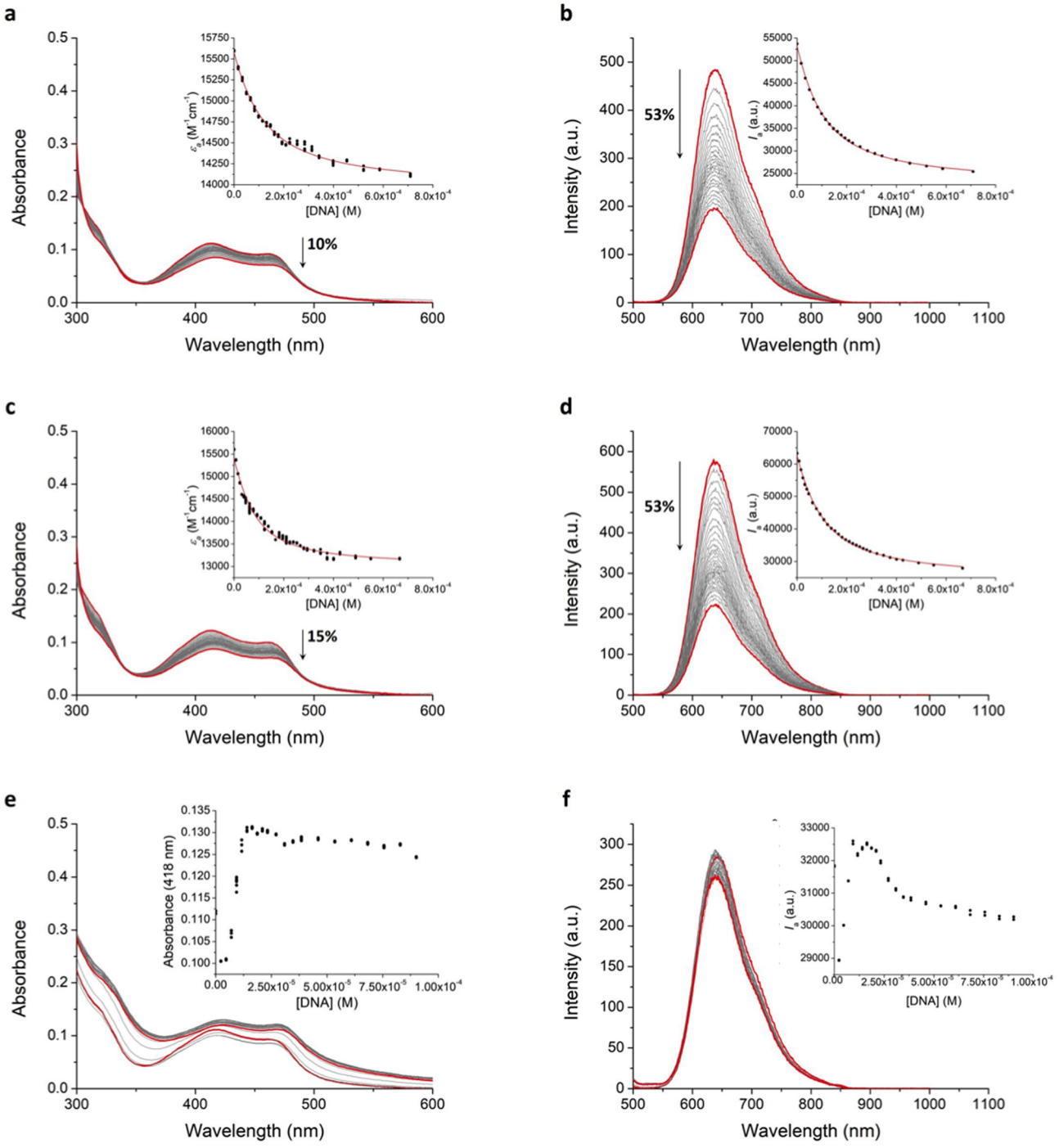

Figure 6. Changes in the UV−vis absorption and emission spectra of (a, b) **4** (7.16 μM, λ_{exc} = 414 nm), (c, d) **5** (7.85 μM, λ_{exc} = 413 nm), and (e, f) **6** (7.03 μM, λ_{exc} = 418 nm) with increasing concentration of stDNA (0−710, 0−666, and 0−90 μM, respectively) in 10 mM sodium phosphate-buffered aqueous solution at pH 7.4. Inset: Plot of ε_a (M^{-1} cm^{-1}) or I_a (a.u.) vs [DNA] (M, bases) using data from absorbance at (a) 414, (c) 413, and (e) 418 nm or integrated MLCT emission intensity (b, d, f) and the best fit of the data, when possible, using a modification of the Bard equation.

stDNA, and then an increase up to 1.1 equiv of stDNA (Figure 5f). This was then followed by a decrease in the emission intensity until a plateau was reached. For both complexes, the maximum of emission intensity was blue-shifted by ca. 7 nm.

Complexes **4**−**6**, containing the TAP moiety, also exhibited significant changes in their photophysical properties upon addition of stDNA (Figure 6). Here, **4** and **5** displayed a 10% and 15% hypochromism in the MLCT band at 414 and 413 nm, respectively (Figure 6a,c). The emission titrations of **4** and **5** with stDNA showed a quenching of the MLCT emission intensity at 636 nm by 53% for both complexes (Figure 6b,d), following the trend observed for Ru(II) polypyridyl complexes containing at least two π-deficient TAP ligands for which their excited state is quenched as a consequence of a photoinduced electron transfer between the guanine moieties contained by the DNA and the MLCT excited state of the complex.[51,52,63]

As was seen for the phen analogue **3** above, the TAP complex **6** showed an initial decrease in the absorption at the

https://doi.org/10.1021/acsabm.1c00284
ACS Appl. Bio Mater. XXXX, XXX, XXX−XXX

Table 3. DNA Binding Parameters of 1, 2, 4, and 5[a] Calculated from Fits to Absorbance and Emission Data in 10 mM Sodium Phosphate-Buffered Aqueous Solution at pH 7.4, at 298 K

	absorption			emission		
complex	K_b (10^4 M^{-1})[b]	n (base pairs)[b]	R^2	K_b (10^4 M^{-1})[b]	n (base pairs)[b]	R^2
1	42 ± 8	3.6 ± 0.3	0.99	34 ± 2	3.4 ± 0.1	0.99
2	553 ± 99	3.5 ± 0.3	0.99			
4	8.1 ± 0.4	3.5[c]	0.99	9.4 ± 0.5	3.5	0.99
5	15 ± 2	3.5[c]	0.98	9.7 ± 0.3	3.5	0.99

[a]No results for **3** and **6**. [b]Results correspond to the mean ± SEM. [c]n (base pairs) is fixed to 3.5, as the weak binding of the complex to DNA did not allow to keep n as a free parameter.

MLCT band upon the addition of 0.3 equiv of stDNA, followed by a strong enhancement up to 2.0 equiv of stDNA (Figure 6e). Thereafter, a slight decrease was observed until the absorption reached a plateau. It is possible that this initial drop could be due to breakup of some degree of self-assemblies that are initially formed for **6** upon initial DNA addition. A red shift of ca. 6 nm was concomitantly observed in the MLCT band. The MLCT emission was also monitored, and, unexpectedly, the typical quenching seen for such complexes was not observed for **6** (Figure 6f). In contrast, **6** exhibited a triphasic behavior consisting of an initial strong quenching in the MLCT emission intensity centered at 643 nm after the addition of 0.3 equiv of stDNA, which was then followed by an emission enhancement up to the addition of 2.3 equiv of stDNA. After this a decrease was observed in the emission intensity upon further addition of stDNA until no more changes were observed (i.e., a plateau was observed). These changes were accompanied by a less obvious blue shift of ca. 4 nm.

From the above spectroscopic changes, the binding parameters such as the binding constant (K_b) and the binding size (n) for some of these complexes were calculated using a modified Bard et al. model.[68,69] The plots of ε_a vs [DNA] and the corresponding best fit of the data, when possible, as well as the I_a vs [DNA], are shown as insets in Figures 5 and 6 for the two types of systems. The values of the obtained binding parameters are summarized in Table 3. A first observation of the values determined from these titrations revealed a higher affinity of the phen complexes (**1** and **2**) for stDNA when compared with their TAP analogues (**4** and **5**), and a difference of 1 order of magnitude was found for complexes containing the same *N*-1,10-phenanthrolin-5-yl-alkylamide ligand and either phen or TAP as ancillary ligands. Thus, **1** and **4** exhibited K_b values in the order of 10^5 and 10^4 M^{-1}, respectively, while **2** and **5** showed K_b values in the order of 10^6 and 10^5 M^{-1}, respectively. This behavior could be anticipated from the fact that TAP complexes displayed a smaller hypochromic effect in their MLCT band upon addition of stDNA than phen complexes and a lower curvature of the titration curve. This might be due to partial intercalation of the phen ligands between the DNA base pairs or their location within the minor groove.[70,71] While we were able to determine the binding size n as ca. 3.5 base pairs for the phen-based complexes, in the case of the TAP complexes (due to their relatively weak DNA binding) n could not be kept as a free parameter when the spectroscopic data were analyzed. Hence, it was necessary to fix these as 3.5 by assuming that both the phen and the TAP systems have similar binding sizes. Unfortunately, DNA binding parameters for **3** and **6** containing the 21 carbon alkyl chain could not be determined as a result of their complicated spectroscopic behavior in the presence of stDNA.

From these titration experiments, it is clear that the presence of the alkyl chain improved the affinity of the complexes for DNA since larger K_b values were observed for **2** and **5** when compared with their short chain analogues **1** and **4**. At the same time, **3** and **6** gave rise to more complex binding interactions which could not be elucidated using the classic Bard et al. binding model. These results suggest that additional hydrophobic interaction could also occur and contribute to the DNA binding event of such complexes as it was previously discussed in the literature for cationic surfactants.[46,72−76]

Thermal Denaturation (T_m) and Circular Dichroism Studies. Having investigated the DNA binding of **1**−**6** by probing the complexes' ground- and excited-state properties above, we also examined their ability to stabilize or destabilize the DNA upon their binding by carrying out both thermal denaturation (T_m) and circular dichroism (CD) studies.[77] The thermal denaturation studies were carried out using stDNA in 10 mM sodium phosphate aqueous buffer at pH 7.4, by monitoring the changes in the absorbance at 260 nm of stDNA (150 μM) in the presence of **1**−**6**, respectively, at DNA phosphate-to-ruthenium dye (P/D) ratios of 50, 20, and 10, while the temperature was gradually increased from 30 to 90 °C. Experiments were repeated at least three times to ensure reproducibility. The resulting thermal denaturation curves recorded in the presence of **1**−**6** at a P/D ratio of 10 (Figure 7) demonstrate the ability of the complexes to stabilize the DNA helix decrease with increasing alkyl chain length, the T_m being determined as 69.1 °C for stDNA alone. While **1**−**6** do not contain π-extended aromatic ligands, which normally favor binding to DNA by intercalation, the other binding modes such as groove binding or partial intercalation are still possible and both give rise to stabilization in the DNA double helix. At P/D of 50, the acetamide-based complexes **1** and **4** were shown to slightly increase (less than 1 °C) the T_m of stDNA (Figure S26a,b and Table S4, Supporting Information). However, at a P/D of 20, more appreciable changes were observed, resulting in T_m values of 5.0 and 2.6 °C, respectively. In contrast, at a P/D ratio of 10, these complexes were found to further increase T_m significantly to 10.4 and 6.2 °C, respectively, demonstrating their binding to DNA. No significant changes in the stDNA T_m were observed for **2**, **3**, **5**, and **6** at P/D ratios of 50 and 20 (Figure S26c−f and Table S4, Supporting Information). However, at a P/D of 10, **2** and **5**, containing the 10 carbon alkyl chain, displayed a slight increase in the stDNA T_m of 2.1 and 2.6 °C, respectively. In contrast, **3** and **6** did not induce a significant increase in the stDNA T_m and, therefore, it can be concluded that their binding interactions do not stabilize the DNA double-helix structure. This is in agreement with the results obtained from

https://doi.org/10.1021/acsabm.1c00284
ACS Appl. Bio Mater. XXXX, XXX, XXX−XXX

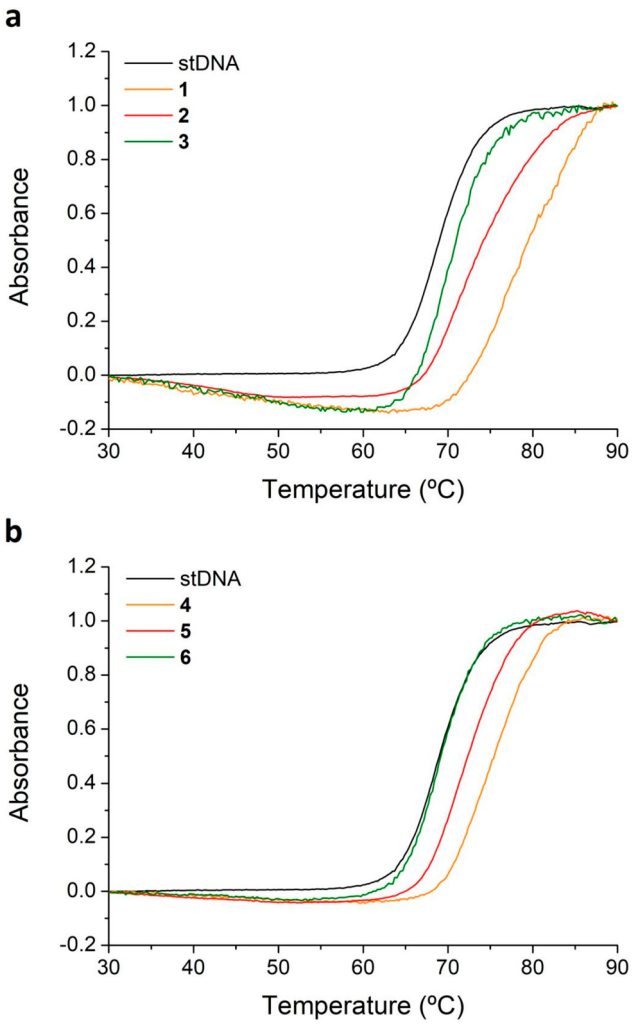

Figure 7. Thermal denaturation curves of stDNA (150 μM) in 10 mM sodium phosphate-buffered aqueous solution at pH 7.4, in the absence and presence of (a) **1**–**3** and (b) **4**–**6** at a P/D ratio of 10.

the ground- and the excited-state investigations, which demonstrated that **3** and **6** interact with stDNA in a nonclassic manner due to their long alkyl chain lengths. Hence, in order to shed more light on the binding of these complexes to DNA, circular dichroism (CD) studies were also carried out.

CD titrations of stDNA with **1**–**6** were performed in 10 mM sodium phosphate aqueous buffer at pH 7.4. Here, the concentration of stDNA was kept constant (150 μM) and the concentration of these complexes was varied to give P/D ratios of 50, 20, 10, and 5. All of the titrations were repeated at least three times to ensure reproducibility. Overall, these results showed that the CD spectrum of stDNA was affected by the presence of all of these complexes. However, these changes were mainly within the UV regions, where the absorption bands of complexes and DNA overlap. In the presence of **1** and **4** at higher loadings (e.g., P/D of 5), the appearance of a negative band was observed in the DNA absorption region with a maximum at approximately 293 nm for both complexes, which corresponds to the π–π^* intraligand transitions of the ancillary phen and TAP ligands (Figure S27a,b, Supporting Information). Hence, it is difficult to state with certainly if these bands result from an induced CD (ICD) or are due to structural changes in the DNA as a result of these complexes interacting with the double-helix structure through groove binding, or partial or full intercalation. However, these changes are similar to what we have previously seen in our investigations, which demonstrate that they are due to the association of these complexes with DNA.[33,34,69] Similarly, the CD spectra of stDNA obtained in the presence of **2** and **5** showed the evolution of a negative band at 285 and 296 nm, respectively (Figure 8). In addition, the phen derivative **2** also

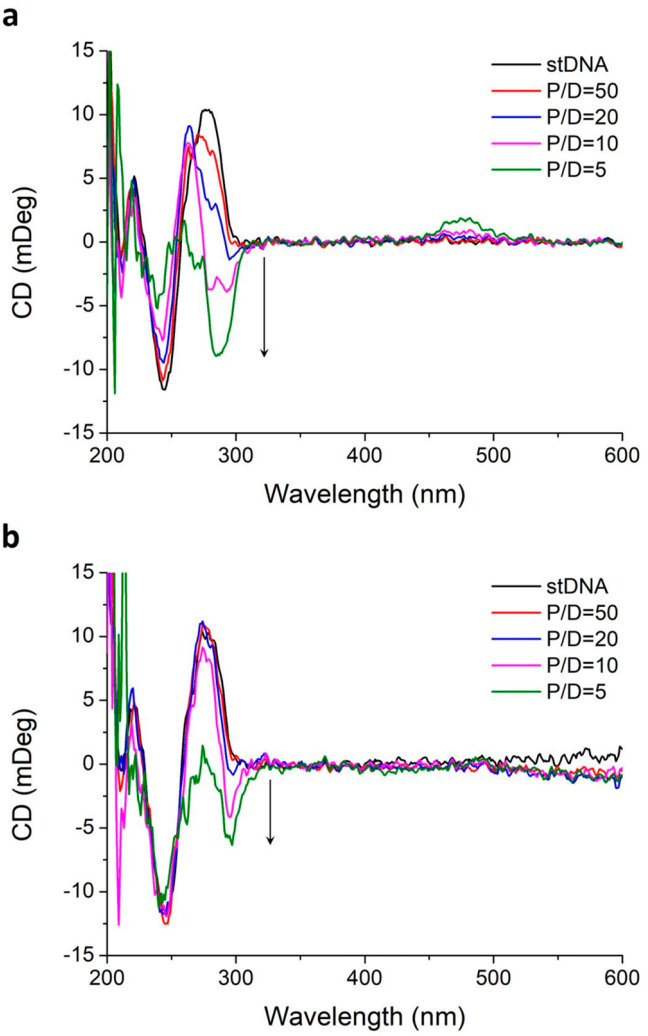

Figure 8. Circular dichroism spectra of stDNA (150 μM) in 10 mM sodium phosphate-buffered aqueous solution at pH 7.4, in the absence and presence of (a) **2** and (b) **5** at different P/D ratios.

exhibited a small positive ICD signal at about 475 nm that can be attributed to the typical MLCT absorption band. In contrast to these results, and in agreement with that seen above, only minor changes were observed upon addition of **3** and **6** to stDNA with only a small negative band in the UV region being observed, resulting in an almost complete disappearance of the characteristic DNA CD signal at a P/D ratio of 5 (Figure S27c,d, Supporting Information). Once again, the phen derivative **3** showed a small positive ICD signal at ca. 480 nm in the charge-transfer region.

Taking into account the previous spectroscopic studies outlined above, we can conclude that **1**, **2**, **4**, and **5** bind to DNA through interactions that are likely a combination of both electrostatic attraction (between the cationic Ru(II) complex and the negatively charged phosphate backbone of

https://doi.org/10.1021/acsabm.1c00284
ACS Appl. Bio Mater. XXXX, XXX, XXX−XXX

DNA) and a partial intercalation into the DNA base pairs (or insertion into the grooves of the ancillary ligands), as has been demonstrated in the literature.[70,71] However, in the case of **3** and **6**, it can be anticipated that, in addition to the above binding modes, additional hydrophobic interactions exist. However, as discussed above, both **3** and **6** exhibited complicated spectroscopic behavior upon addition of DNA, which meant that K_b values could not be determined for these complexes, and hence, the strength of their interaction with DNA could not be quantified. Furthermore, the above DNA denaturation and CD studies have shown that, for both **3** and **6**, no significant stabilization nor changes in the conformation of the DNA helical structure occur, which would suggesting a low affinity of complexes for both **3** and **6** for stDNA.

Lipophilicity and Cellular Uptake Studies. Lipophilicity plays a key role in the cellular uptake mechanism of molecules designed to be used in a cellular environment and can strongly influence their cytotoxicity and cellular localization.[35] In this context, the gradual increase in the length of the alkyl chain is expected to make the complexes herein more lipophilic and improve their ability to cross the cell membrane compared to $[Ru(phen)_3]^{2+}$ or $[Ru(TAP)_2phen]^{2+}$. Therefore, the logarithm of the partition coefficient (log *P*) between octanol and water was evaluated for **1**, **2**, **4**, and **5** using the "shake-flask" method,[78] with the log *P* values of $[Ru(phen)_3]^{2+}$, **3**, $[Ru(TAP)_2phen]^{2+}$, and **6** also included for comparison (Table 4).[48] Both the alkyl chain length and the ancillary ligands coordinated to the Ru(II) center showed influence on the lipophilicity of the complexes. Thus, the log *P* values obtained for **1**−**3** containing phen as ancillary ligands exhibited an enhancement of the lipophilicity with the increasing alkyl chain length. In this manner, **3**, containing a 21 carbon alkyl chain, displayed the highest lipophilicity with a log *P* value of 1.07, followed by **2**, with a 10 carbon alkyl chain and a log *P* value of −1.40. On the other hand, $[Ru(phen)_3]^{2+}$ and **1**, containing the acetamide functionalized phen ligand, were found to be the least lipophilic complexes with log *P* values of −2.28 and −2.52, respectively. Modulation of the lipophilicity of Ru(II) polypyridyl complexes by varying the number of methylene groups contained by the polypyridyl ligands have already been reported by researchers in the literature.[79]

Table 4. log *P* Values of 1, 2, 4, and 5 at 298 K and Their Corresponding IC_{50} Values in HeLa Cells Both in the Dark and with Exposure to Light[a]

complex	log *P*[b]	IC_{50} dark (μM)[b]	IC_{50} light (μM)[b]	PI[c]
$[Ru(phen)_3]^{2+}$[d]	−2.28 ± 0.12	>100	>100	
1	−2.52 ± 0.08	>100	>100	
2	−1.40 ± 0.05	38 ± 7	9 ± 4	4
3[d]	1.07 ± 0.08	13 ± 2	0.47 ± 0.01	27
$[Ru(TAP)_2phen]^{2+}$[d]	−2.76 ± 0.02	>100	31 ± 3	>3
4	−2.76 ± 0.22	>100	15 ± 2	>7
5	−1.97 ± 0.05	14 ± 4	9 ± 2	2
6[d]	0.49 ± 0.07	11 ± 3	2 ± 1	6

[a]Complexes $[Ru(phen)_3]^{2+}$, **3**, $[Ru(TAP)_2phen]^{2+}$ and **6** are included for comparison.[48]. [b]log *P* and IC_{50} values correspond to the mean ± SEM. [c]Phototoxic index (PI) is defined as the ratio of the IC_{50} value in the dark to the IC_{50} value upon light irradiation. [d]Estalayo-Adrián et al.[48]

A similar behavior was observed for the TAP analogues **4**−**6**. Thus, while **6** and **5**, with 21 and 10 carbon alkyl chains, respectively, showed the highest log *P* values, 0.49 and −1.97, respectively, both $[Ru(TAP)_2phen]^{2+}$ and **4**, containing only one methyl group, displayed the lowest log *P* values, −2.76 in both cases. Furthermore, complexes containing phen as ancillary ligands were shown to be more lipophilic than those containing TAP. It has been demonstrated that substitution of phen ancillary ligands by 2,2′-bipyridine (bpy) results in a significant reduction in the lipophilicity of the complex.[80] However, to the best of our knowledge, log *P* values of TAP-containing complexes have only been reported by us previously,[48] although ICP-MS measurements have demonstrated that $[Ru(phen)_3]^{2+}$ tethered to the cell-penetrating peptide TAT exhibited a greater uptake in HeLa cells than its TAP analogue.[23] This suggests that TAP complexes are more hydrophilic than their phen analogues, which is in agreement with the results presented here for complexes $[Ru(phen)_3]^{2+}$, $[Ru(TAP)_2phen]^{2+}$, and **1**−**6**.

Cellular uptake of **1**, **2**, **4**, and **5** in HeLa cervical cancer cells was then investigated and compared to that observed for $[Ru(phen)_3]^{2+}$, **3**, $[Ru(TAP)_2phen]^{2+}$, and **6** in our previous study.[48] Thus, HeLa cells were incubated with **1** and **4** (50 μM) at 37 °C for 24 h and **2** and **5** (10 μM) at 37 °C for 2, 4, and 24 h before being imaged using confocal fluorescence microscopy (Figure 9). As expected, an increase of the alkyl chain length has a positive effect on the cellular uptake of these complexes, this being in agreement with the lipophilicity studies discussed above. In the same manner as $[Ru(phen)_3]^{2+}$ and $[Ru(TAP)_2phen]^{2+}$, **1** and **4**, containing the acetamide functionalized phen ligand, were not taken up into the cells and luminescence from these complexes could only be imaged in the medium under high-powered laser, with little or no luminescence inside the cells. However, as was previously reported[21] for the complexes bearing a 21 carbon alkyl chain, **3** and **6**, time-dependent cellular uptake was observed for **2** and **5** with a 10 carbon alkyl chain. These complexes were taken up into the cells after 2 h incubation with an increase of their cellular uptake observed after 4 and 24 h incubation, as evidenced by increasing the red luminescent emission from these complexes within the cytoplasm of the cells (Figure S28, Supporting Information).

Furthermore, it should be pointed out that **5** showed a very weak luminescence inside the cells compared to that seen for **2**, **3**, and **6**. A reduction in the emission intensity of the Ru(II) TAP complexes in the cellular environment when compared to their phen analogues has also been reported by other authors in the literature.[23,24] It is well-known that Ru(II) complexes containing at least two π-acceptor ligands, such as TAP, are strong enough oxidizing agents to extract an electron from weakly reducing biomolecules (e.g., guanine or tryptophan) through a PET process, resulting in a quenching of the luminescence of the metallic complex.[63,64] In this context, it can be presumed that the luminescence of **5** is quenched by a PET process between the Ru(II) moiety and the amino acids residues of the proteins existing within the cell. Although the same behavior could be expected for **6**, the longer alkyl chain might prevent the metallic center from being in close proximity to the reducing species and protect its luminescence from being quenched.

To further understand the luminescence properties of these complexes in a biological environment, emission studies of the TAP complexes **5** and **6** in the presence of L-tryptophan were carried out. The same studies were conducted for **2** and **3** for comparison. The emission spectra of the four complexes (10

https://doi.org/10.1021/acsabm.1c00284
ACS Appl. Bio Mater. XXXX, XXX, XXX−XXX

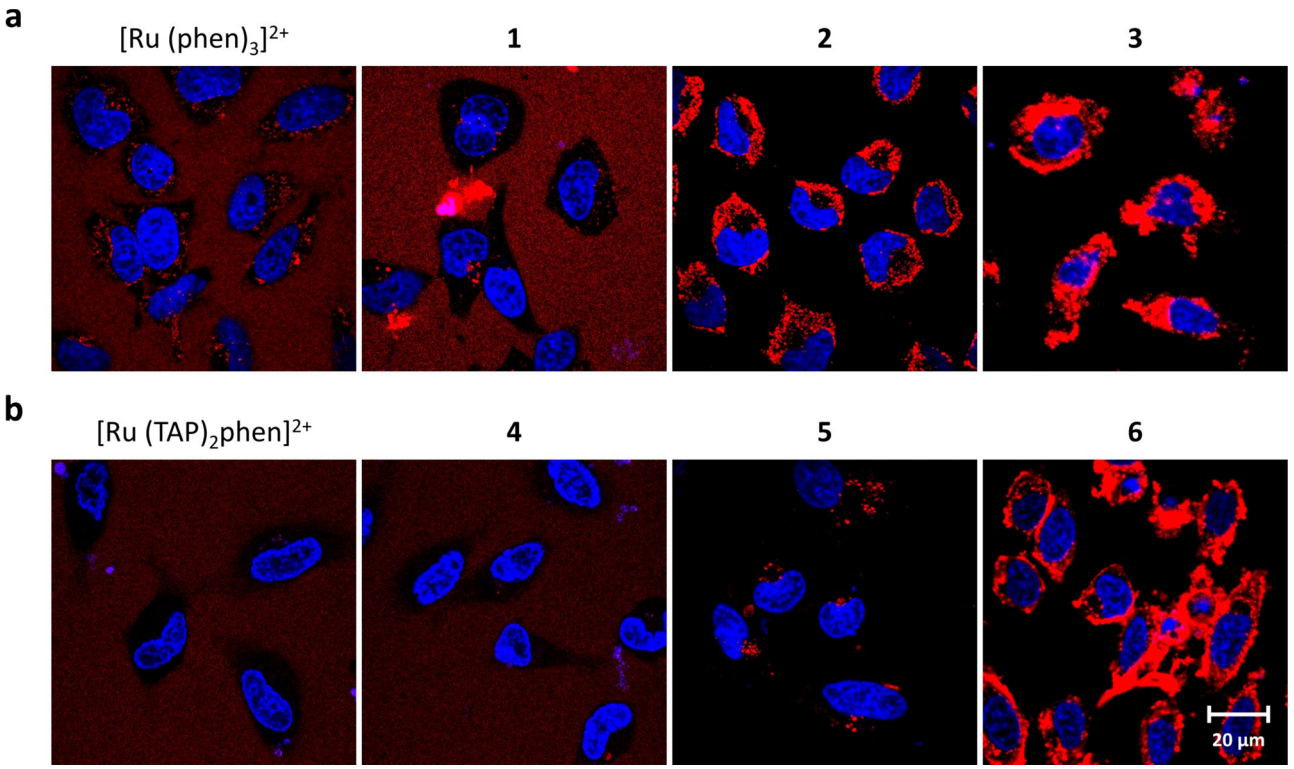

Figure 9. Confocal fluorescence microscopy images of HeLa cells showing the uptake of (a) $[Ru(phen)_3]^{2+}$ (50 μM), **1** (50 μM), **2** (10 μM), and **3** (10 μM) and (b) $[Ru(TAP)_2phen]^{2+}$ (50 μM), **4** (50 μM), **5** (10 μM), and **6** (10 μM) after 24 h incubation. The nucleus is stained blue with Hoechst 33258.

μM) in the absence or in the presence of L-tryptophan (5 mM) were recorded (Figure S29, Supporting Information). Emission intensities of the phen complexes **2** and **3** decreased by 9 and 35% at 603 and 614 nm, respectively, in the presence of L-tryptophan. Interestingly, both **5** and **6** showed similar luminescence quenching in the presence of L-tryptophan with an 89 and 91% decrease in emission at 636 and 643 nm, respectively. Therefore, it may be presumed that, although both complexes exhibited a decrease of the emission in the presence of the reducing amino acid, the higher lipophilicity of **6**, when compared to **5**, results in a larger intracellular concentration and, consequently, in a higher emission intensity despite the luminescence quenching by reducing amino acids residues of the proteins within the cell.

Cellular Toxicity Studies. In order to elucidate the role of the alkyl chain length in the ability of these complexes to reduce cell viability, the cytotoxic potentials of **1**, **2**, **4**, and **5** in HeLa cells were evaluated using the Alamar Blue assay and compared to those observed for $[Ru(phen)_3]^{2+}$, **3**, $[Ru(TAP)_2phen]^{2+}$, and **6** in our previous study.[48] Because these complexes were shown to produce singlet oxygen, their ability to induce cytotoxicity after light activation was also studied. Therefore, cells were treated with **1**, **2**, **4**, and **5** for 24 h before being either irradiated with 18 J cm^{-2} of light for 1 h using a UV-filtered Hg–Xe arc lamp or kept in the dark. Cells were incubated for a further 23 h followed by addition of the Alamar Blue dye and assessment of the cytotoxicity (Table 4 and Figure S30, Supporting Information). As expected from the lack of cellular uptake observed by confocal microscopy and in the same manner as $[Ru(phen)_3]^{2+}$ and $[Ru(TAP)_2phen]^{2+}$, **1** and **4**, containing the acetamide functionalized phen ligand, did not induce any cytotoxicity in the HeLa cells in the dark up to a concentration of 100 μM, and as such, IC_{50} values could not be determined for these complexes. However, both $[Ru(TAP)_2phen]^{2+}$ and **4** were found to be slightly toxic after light activation with IC_{50} values of 31 and 15 μM, respectively. It has been demonstrated that light exposure can facilitate the cellular internalization of some Ru(II) complexes as their ability to generate $^1O_2$ can increase the cell membrane permeability.[36,81−83]

To further study the effect of light in the cellular uptake, HeLa cells were treated with $[Ru(TAP)_2phen]^{2+}$ or **4** (50 μM) before being irradiated for 1 h and incubated for a further 2 h (Figure S31, Supporting Information). HeLa cells, incubated with either complex in the dark for 3 h, were used as a control. No change in the cellular uptake of any of the complexes was observed upon light activation. However, while HeLa cells containing $[Ru(TAP)_2phen]^{2+}$ remained unaltered, evidence of increased toxicity of **4** after light irradiation was found in cell morphology changes compared to the ones in dark conditions. This was in agreement with the lower IC_{50} value observed for **4** after light activation when compared with that obtained for $[Ru(TAP)_2phen]^{2+}$. These results demonstrate that a photo-induced cell membrane permeabilization is not the reason for the phototoxicity observed for $[Ru(TAP)_2phen]^{2+}$ or **4**. Moreover, although both derivatives $[Ru(phen)_3]^{2+}$ and **1**, which instead contain phen as ancillary ligands, were shown to generate more $^1O_2$, these complexes did not display any toxicity in HeLa cells after light irradiation. As was suggested for $[Ru(TAP)_2phen]^{2+}$ in our previous study,[48] the phototoxicity observed for **4** should not be related to the Type-II photosensitization effect as this complex produce less $^1O_2$ than **1**, but maybe due to their additional Type-I photosensitization

https://doi.org/10.1021/acsabm.1c00284
ACS Appl. Bio Mater. XXXX, XXX, XXX−XXX

mechanism (PET) because of its highly oxidizing character in the excited state.[63,64]

In contrast to these results, **2** and **5**, with a 10-carbon alkyl chain, displayed modest IC_{50} values against HeLa cells of 38 and 14 μM, respectively, after 48 h incubation in the absence of light. Some increase in cytotoxicity was observed after they were exposed to visible light, both complexes showing IC_{50} values of 9 μM which corresponds to a phototoxic index (PI) of ca. 4 and 2, respectively. Similarly, in our previous work we reported IC_{50} values of 13 and 11 μM in dark condition for **3** and **6**, respectively,[48] which contain a 21 carbon alkyl chain. After photoactivation, IC_{50} values of 0.47 and 2 μM were observed for **3** and **6**, respectively, which correspond to PIs of ca. 27 and 6, revealing **3** as a promising light-activated therapeutic agent.

As was demonstrated above, having a long alkyl chain increases the lipophilicity of these complexes and makes them more efficiently internalized into cells. This results in a larger intracellular concentration of the Ru(II) complex, which explains the increase of the IC_{50} values with the length of the alkyl chain. Likewise, the photoactivation observed for **2**, **3**, **5**, and **6** is in agreement with their previously demonstrated ability to produce $^1O_2$ or other ROS.[48] Therefore, these results demonstrate that the toxicity observed in the dark is due to the increasing length of the alkyl chain, while the ruthenium core provide the resulting complexes with the ability to be photoactivated.

CONCLUSIONS

In this study, we have reported a family of six Ru(II) polypyridyl complexes in which the metal center was coordinated to either phen (**1**–**3**) or TAP (**4**–**6**) as ancillary ligands and where the third ligand consisted of a different length of alkylamide functionalized phen. The effect of the alkyl chain length on the photophysical, photochemical, and photobiological properties of these complexes was evaluated. No significant changes were observed in the absorption and emission properties of the complexes containing either the acetamide functionalized phenanthroline ligand, **1** and **4**, or the 10 carbon alkyl chain, **2** and **5**, when compared to the well-known complexes $[Ru(phen)_3]^{2+}$ and $[Ru(TAP)_2phen]^{2+}$. However, the extension of the alkyl chain to 21 carbons seemed to affect both the luminescence quantum yields and lifetimes of complexes **3** and **6**, most likely due to their ability to self-assemble in solution as a result of their amphiphilic character. In addition, the luminescence lifetime of **3** was found to rise upon increasing the complex concentration, while the opposite effect was observed for **6**, indicating different photophysical responses to the self-assembly process by the phen (**3**) and TAP (**6**) complexes, due in part to oxygen quenching protection and self-quenching of their excited states.

Direct measurement of $^1O_2$ phosphorescence at 1265 nm in O_2-saturated D_2O revealed an effect of the alkyl chain length on the ability of **1**–**6** to produce $^1O_2$. Thus, while **1**, **2**, **4**, and **5** showed moderate $^1O_2$ photosensitization in air-saturated H_2O, very low quantum yield values of $^1O_2$ were obtained for **3** and **6**. Efforts were made to indirectly quantify the $^1O_2$ production by **3** and **6** by monitoring the fluorescence disappearance of the water-soluble $^1O_2$ chemical probe ABDA, as this method allowed one to work in a concentration range where the complexes are expected to behave as free monomers, facilitating their interaction with molecular oxygen. However, no conclusive results were obtained from these experiments probably due to hydrophobic interaction between the highly lipophilic complexes and the probe.

The DNA binding ability of these complexes was also evaluated. We show that while **1**, **2**, **4**, and **5** all give rise to classic changes in their photophysical properties, where changes in both the absorption and emission spectra could be analyzed to give their affinity (binding constants) and binding size, those observed for **3** and **6** were complex, so that we were unable to treat the data in a meaningful way to determine binding parameters.

In vitro studies of complexes **1**–**6** in HeLa cervical cancer cells were then performed in order to probe the applicability of these complexes in live systems. Confocal fluorescence microscopy revealed the influence of the alkyl chain length on the cellular internalization and thus **2**, **3**, **5**, and **6**, containing long alkyl chains, were shown to be rapidly taken up into the cells with a preliminary localization in the cell membrane while **1** and **2** were not internalized by the cells as was found for $[Ru(phen)_3]^{2+}$ and $[Ru(TAP)_2phen]^{2+}$. This is in agreement with the log *P* values determined for these complexes, where an increase of the lipophilicity with the alkyl chain length was observed, **3** and **6** being the most lipophilic complexes.

Finally, cellular toxicity studies showed that complexes **2**, **5**, and **6** displayed moderate phototoxicity against HeLa cells in contrast to **3** which exhibited significant light-dependent cytotoxicity with a PI of ca. 27, revealing a potential for its use as a light-activated therapeutic agent. In conclusion, this work demonstrates that the cellular uptake and phototoxicity of Ru(II) polypyridyl complexes can be modulated by carefully selecting the ancillary ligands (phen or TAP) and the alkyl chain length of the lipophilic ligands coordinated to the ruthenium center.

EXPERIMENTAL SECTION

Materials and Instrumentation. All chemicals and solvents were obtained commercially and, unless specified, used without further purification. Solvents for synthetic purposes were used at general purpose reagent (GPR) grade unless otherwise stated. Dry solvents were obtained from a solvent purification system (SPS) purchased from Innovative Technology Inc.

General Characterization Techniques. All NMR spectra were recorded using either a Bruker Avance III 400 NMR spectrometer operating at 400 MHz for ^1H NMR and 101 MHz for ^{13}C NMR or a Bruker Avance II 600 NMR spectrometer operating at 600 MHz for ^1H NMR and 151 MHz for ^{13}C NMR. Chemical shifts (δ) were referenced relative to the internal solvent signals. Electrospray ionization (ESI) mass spectra were recorded on a Micromass LCT spectrometer (calibrated using leucine enkephalin m/z = 556.2771). Matrix-assisted laser desorption/ionization (MALDI) mass spectra were recorded on a MALDI QToF Premier (Waters Corp., Micromass MS Technologies, Manchester, U.K.), and high-resolution (HR) mass spectra were determined by a peak matching method using Glu-Fib as an internal reference (m/z = 1570.677). Infrared spectra were recorded on a PerkinElmer Spectrum One FT-IR spectrometer fitted with a Universal ATR Sampling Accessory for solid samples. Melting points were determined using an IA9000 digital melting point apparatus. Elemental analyses were conducted at the Microanalytical Laboratory, School of Chemistry, University College Dublin (UCD).

Photophysical Characterization. UV–vis absorption spectra were recorded on a Varian CARY 50 spectrophotometer. Emission and excitation spectra were recorded on a Varian Carey Eclipse fluorimeter. Luminescence quantum yields (Φ_{em}) were determined using an established method.[48,58] Luminescence lifetimes were measured by single-photon timing on a Horiba Fluoromax-4TC-

https://doi.org/10.1021/acsabm.1c00284
ACS Appl. Bio Mater. XXXX, XXX, XXX–XXX

SPC or a Fluorolog FL 3−22 equipped with a FluoroHub v2.0 single-photon timing module.

Direct Detection of Singlet Oxygen (Time-Resolved Near-Infrared Phosphorescence). Quantum yields of singlet oxygen production were measured using an Edinburgh Instruments (U.K.) LP-900 laser kinetic spectrometer system equipped with a frequency-doubled Nd:YAG laser (Minilite II, Continuum, CA) and a Hamamatsu H10330-45 NIR PMT module for the singlet oxygen emission monitoring at 1265 nm (Bentham TM300 monochromator with 600 grooves mm^{-1} NIR grating). Absorbance matched ($A_{532} \approx 0.40$) solutions of the ruthenium complex and the reference photosensitizer $[Ru(phen)_3]Cl_2$ ($\Phi_\Delta = 0.39 \pm 0.03$ in O_2-saturated D_2O at room temperature). Full details have been previously given.[48,59] All $^1O_2$ luminescence decay profiles were fitted using a single-exponential function [after excluding the fast (sub-μs) decay due to the residual Ru(II) sensitizer emission even under O_2 saturation of the solution].[59,84] From the experimental data obtained in D_2O, the Φ_Δ values in air-equilibrated H_2O were calculated taking into account eqs 1 and (2):[55]

$$P_{O_2}^{T} = \tau k_q [O_2] = 1 - \frac{\tau}{\tau_0} \quad (1)$$

$$\Phi_\Delta = \Phi_T P_{O_2}^{T} f_\Delta^{T} \quad (2)$$

Φ_T is considered to be equal to 1 for these types of complexes.[55] Assuming that f_Δ^T is the same in O_2-saturated D_2O and air-saturated H_2O, then Φ_Δ values in air-equilibrated H_2O were determined using eq 3,:

$$\Phi_{\Delta,H_2O,air}^{complex} = \Phi_{\Delta,D_2O,O_2}^{complex}\left(1 - \frac{\tau_{H_2O,air}}{\tau_{H_2O,Ar}}\right)\Big/\left(1 - \frac{\tau_{D_2O,O_2}}{\tau_{D_2O,Ar}}\right) \quad (3)$$

Indirect Detection of Singlet Oxygen (Photo-oxidation of a Chemical Probe). Singlet oxygen production was also evaluated using the water-soluble $^1O_2$ trap ABDA.[48,85]

Partition Coefficients (log P). Partition coefficients were determined by the shake-flask method. The log P values were calculated according to a method previously employed in our research group.[48]

$$\log P = \log\left(\frac{c_t - c_{water}}{c_{water}}\right)$$

DNA Binding Studies Techniques. UV−vis absorption and emission titrations were carried out on samples of the dye at $(1 \pm 0.5) \times 10^{-5}$ M at 298 K by monitoring changes in the absorption and emission spectra of the complexes in 10 mM sodium phosphate buffer (pH 7.4) upon successive additions of aliquots of stDNA. The results are quoted using the concentration of stDNA expressed as a nucleotide phosphate-to-dye ratio (P/D ratio). Binding constants (K_b) and binding size (n) were determined using a reorganization of the original Bard et al. equation. K_b values represent the mean ± SEM of three independent experiments.

General Biological Procedures. *Cell Culture.* HeLa cells were grown in a cell culture flask using Dulbecco's modified Eagle medium supplemented with 10% fetal bovine serum, 1% penicillin/streptomycin, and 0.2% plasmocin at 37 °C in a humidified atmosphere of 5% CO_2.

Confocal Microscopy. HeLa cells were seeded at a density of 5×10^4 cells/mL and treated as indicated. Cells were then washed using a known protocol[48] and imaged by live microscopy using an Olympus FV1000 point scanning microscope with a 60× oil immersion lens (NA, 1.42).

Viability Assays. HeLa cells were seeded at a density of 2.5×10^3 cells/mL in a 96-well plate and treated with different concentrations of the appropriate Ru(II) complex. Into each well 20 μL of Alamar Blue (BioSource) was added and left to incubate at 37 °C in the dark for 4 h. Fluorescence was read at 590 nm using a fluorescence microplate reader (SpectraMax Gemini XS, Molecular Devices; λ_{exc} = 544 nm). Data points represent the mean ± SEM of triplicate treatments performed on three independent days. For photoactivation studies, cells were illuminated with 18 J cm^{-2} of light for 1 h using a Hamamatsu L2570 200 W Hg−Xe arc lamp equipped with an aqueous solution of $NaNO_2$ as UV filter.

Synthesis and Characterization. 1,4,5,8-Tetraazaphenanthrene (TAP),[86] 5-amino-1,10-phenanthroline,[87] the precursor complexes *cis*-$[Ru(phen)_2Cl_2]$ and *cis*-$[Ru(TAP)_2Cl_2]$,[88] and complexes $[Ru(phen)_3]^{2+}$, $[Ru(TAP)_2phen]^{2+}$, **3**, and **6** were synthesized according to procedures previously reported in the literature.[48]

5-Acetamido-1,10-phenanthroline (7). 5-Amino-1,10-phenanthroline (153 mg, 783 μmol, 1 equiv) and acetic anhydride (0.75 mL, 7.93 mmol, 10 equiv) were mixed in dry MeCN (25 mL). The reaction mixture was stirred in the dark and under an inert atmosphere at room temperature for 2 days. Solvent was removed under reduced pressure, yielding the product as a beige solid which was dried in vacuo (114 mg, 482 μmol, 62%). mp 226−231 °C (decomp.) Lit. mp 230 °C.[87] δ_H (400 MHz, DMSO-d_6): 10.14 (1H, s, NH), 9.13 (1H, dd, H_2, ^3J = 4.2 Hz, ^4J = 1.6 Hz), 9.03 (1H, dd, H_9, ^3J = 4.3 Hz, ^4J = 1.7 Hz), 8.63 (1H, dd, H_4, ^3J = 8.4 Hz, ^4J = 1.7 Hz), 8.44 (1H, dd, H_7, ^3J = 8.2 Hz, ^4J = 1.7 Hz), 8.17 (1H, s, H_6), 7.82 (1H, dd, H_3, ^3J = 8.4 Hz, ^3J = 4.3 Hz), 7.74 (1H, dd, H_8, ^3J = 8.2 Hz, ^3J = 4.3 Hz), 6.13 (3H, s, CH_3). δ_C (101 MHz, DMSO-d_6): 169.49 (C═O), 149.86, 149.29, 145.85 (q), 143.77 (q), 135.81, 131.86 (q), 131.68, 128.10, 124.59 (q), 123.59, 122.84, 119.86, 23.63 (CH_3). ν_{max} (ATR)/cm^{-1}: 3200 (amide N−H stretch), 3040 (aromatic C−H stretch), 2924 (alkane C−H stretch), 1688 (C═O stretch), 1532 (amide N−H bend), 1476 (aromatic C═C stretch), 1420 (C−N stretch). ESI$^+$-HRMS: m/z_{calc} = 238.0980 for $C_{14}H_{12}N_3O$; m/z_{found} = 238.0973 $[M + H]^+$.

N-1,10-Phenanthrolin-5-ylundecanamide (8). 5-Amino-1,10-phenanthroline (101 mg, 516 mmol, 1 equiv) was dissolved in dry CH_2Cl_2 (10 mL), and the solution was cooled to 0 °C before undecanoic acid (108 μL, 516 μmol, 1 equiv), *N*-ethyl-*N*′-(3-(dimethylamino)propyl)carbodiimide hydrochloride (246 mg, 1.28 mmol, 2.5 equiv), and 4-(dimethylamino)pyridine (62.4 mg, 511 μmol, 1 equiv) were added to the solution. The resulting mixture was stirred under inert atmosphere and at 0 °C for 1 h and then for a further 2 days at room temperature. After removing the solvent under reduced pressure, an orange oil was obtained which was dried in vacuo. The addition of H_2O caused precipitation of a beige solid which was isolated by centrifugation and washed several times with more H_2O. The resulting solid was re-dispersed in MeCN, collected by centrifugation, and dried in vacuo, yielding the product as a beige solid (107 mg, 295 μmol, 57%). mp 83−86 °C. δ_H (600 MHz, DMSO-d_6): 10.07 (1H, s, NH), 9.12 (1H, dd, H_2, ^3J = 4.2 Hz, ^4J = 1.6 Hz), 9.03 (1H, dd, H_9, ^3J = 4.2 Hz, ^4J = 1.7 Hz), 8.59 (1H, dd, H_4, ^3J = 8.4 Hz, ^4J = 1.6 Hz), 8.44 (1H, dd, H_7, ^3J = 8.1 Hz, ^4J = 1.7 Hz), 8.17 (1H, s, H_6), 7.82 (1H, dd, H_3, ^3J = 8.4 Hz, ^3J = 4.2 Hz), 7.74 (1H, dd, H_8, ^3J = 8.1 Hz, ^3J = 4.2 Hz), 2.52 (2H, t, $H_{2'}$, ^3J = 7.3 Hz), 1.69 (2H, m, $H_{3'}$), 1.31 (14H, m, $H_{4'}$−$H_{10'}$), 0.84 (3H, t, $H_{11'}$, ^3J = 7.0 Hz). δ_C (151 MHz, DMSO-d_6): 172.44 (C═O), 149.82, 149.26, 145.86 (q), 143.77 (q), 135.75, 131.79 (q), 131.57, 128.09 (q), 124.64 (q), 123.55, 122.78, 119.97, 35.96, 31.30, 28.99, 28.96, 28.81, 28.73, 28.69, 25.22, 22.08, 13.95. ν_{max} (ATR)/cm^{-1}: 3255 (amide N−H stretch), 3046 (aromatic C−H stretch), 2919 and 2849 (alkane C−H stretch), 1655 (C═O stretch), 1543 (amide N−H bend), 1467 (aromatic C═C stretch), 1424 (C−N stretch). ESI$^+$-HRMS: m/z_{calc} = 386.2203 for $C_{23}H_{29}N_3NaO$; m/z_{found} = 386.2206 $[M + Na]^+$.

Bis(1,10-phenanthroline)(N-1,10-phenanthrolin-5-ylacetamide)-ruthenium(II) Chloride (1). The precursor complex *cis*-$[Ru(phen)_2Cl_2]$ (101 mg, 190 μmol, 1 equiv) and ligand 7 (66.7 mg, 281 μmol, 1.5 equiv) were suspended in EtOH/H_2O (1:1, 8 mL). The mixture was deoxygenated by sparging with argon for 15 min and heated at 140 °C for 40 min using microwave irradiation. Solvent was removed at reduced pressure and the resulting solid was purified by alumina chromatography using MeCN/H_2O (10:0 to 9:1) as eluent, yielding the product as a red solid which was dried in vacuo (87.3 mg, 125 μmol, 60%). Calculated for $C_{38}H_{27}N_7Cl_2ORu + 2.3H_2O$: C, 56.27; H, 3.93; N, 12.09; Cl, 8.74. Found: C, 56.21; H, 3.88; N, 12.12; Cl, 8.20. mp 106−109 °C (decomp.). δ_H (400 MHz, CD_3CN):

https://doi.org/10.1021/acsabm.1c00284
ACS Appl. Bio Mater. XXXX, XXX, XXX−XXX

11.61 (1H, s, NH), 9.60 (1H, dd, H_4^{L7}, ^3J = 8.6 Hz, ^4J = 1.1 Hz), 8.64 (1H, s, H_6^{L7}), 8.59 (4H, m, H^{phen}), 8.47 (1H, dd, H_7^{L7}, ^3J = 8.3 Hz, ^4J = 1.1 Hz), 8.25 (2H, s, H_5^{phen} or H_6^{phen}), 8.24 (2H, s, H_5^{phen} or H_6^{phen}), 8.09 (1H, dd, H_2^{L7}, ^3J = 5.2 Hz, ^4J = 1.1 Hz), 8.02 (4H, m, H^{phen}), 7.89 (1H, dd, H_9^{L7}, ^3J = 5.2 Hz, ^4J = 1.1 Hz), 7.62 (5H, m, H_3^{L7} and H^{phen}), 7.52 (1H, dd, H_8^{L7}, ^3J = 8.3 Hz, ^3J = 5.2 Hz), 2.45 (3H, s, CH_3). δ_C (101 MHz, CD_3CN): 171.81 (C═O), 154.17, 153.97, 153.85, 153.80, 153.68, 152.27, 148.87 (q), 137.62, 137.59, 136.94, 135.46, 131.93 (q), 131.88 (q), 128.97, 128.91, 126.85, 126.83, 126.76, 126.74, 126,64, 125.76, 119.79, 24.40 (CH_3). ν_{max} (ATR)/cm^{-1}: 3234 (amide N−H stretch), 3046 (aromatic C−H stretch), 2994 (alkane C−H stretch), 1683 (C═O stretch), 1533 (amide N−H bend), 1480 (aromatic C═C stretch), 1424 (C−N stretch). ESI$^+$-HRMS: m/z $_{calc}$ = 699.1321 for $C_{38}H_{27}N_7ORu$; m/z $_{found}$ = 349.5676 $[M]^{2+}$.

*Bis(1,10-phenanthroline)(N-1,10-phenanthrolin-5-ylundecanamide)ruthenium(II) Chloride (**2**).* Complex **2** was synthesized according to the same procedure described for **1** but using *cis*-$[Ru(phen)_2Cl_2]$ (164 mg, 307 μmol, 1 equiv) as precursor complex and ligand **8** (109 mg, 300 μmol, 1 equiv), yielding the product as a red solid (161 mg, 99.0 μmol, 60%). Calculated for $C_{47}H_{45}N_7Cl_2ORu + 2.6H_2O$: C, 59.88; H, 5.37; N, 10.40; Cl, 7.52. Found: C, 59.57; H, 5.08; N, 10.37; Cl, 7.18. mp 220−223 °C (decomp.). δ_H (400 MHz, CD_3CN): 11.33 (1H, s, NH), 9.48 (1H, dd, H_4^{L8}, ^3J = 8.6 Hz, ^4J = 1.0 Hz), 8.64 (1H, s, H_6^{L8}), 8.60 (4H, m, H^{phen}), 8.47 (1H, dd, H_7^{L8}, ^3J = 8.3 Hz, ^4J = 1.0 Hz), 8.25 (4H, 2s, H_5^{phen} and H_6^{phen}), 8.09 (1H, dd, H_2^{L8}, ^3J = 5.2 Hz, ^4J = 1.0 Hz), 8.02 (4H, m, H^{phen}), 7.90 (1H, dd, H_9^{L8}, ^3J = 5.2 Hz, ^4J = 1.0 Hz), 7.62 (5H, m, H_3^{L8} and H^{phen}), 7.53 (1H, dd, H_8^{L8}, ^3J = 8.3 Hz, ^3J = 5.2 Hz), 2.79 (2H, t, $H_{2'}^{L8}$, ^3J = 7.4 Hz), 1.71 (2H, m, $H_{3'}^{L8}$), 1.34 (14H, m, $H_{4'}$−$H_{10'}^{L8}$), 0.84 (3H, t, $H_{11'}^{L8}$, ^3J = 6.7 Hz). δ_C (101 MHz, CD_3CN): 175.03 (C═O), 154.18, 153.99, 153.88, 153.73, 152.34, 148.89 (q) 137.67, 136.99, 136.08 (q), 135.40, 131.93 (q), 129.03, 128.97, 128.13 (q), 126.91, 126.81, 126.71, 125.85, 119.95, 37.41, 32.61, 30.31, 30.22, 30.03, 26.60, 23.36, 14.37. ν_{max} (ATR)/cm^{-1}: 3243 (amide N−H stretch), 3043 (aromatic C−H stretch), 2922 and 2851 (alkane C−H stretch), 1688 (C═O stretch), 1535 (amide N−H bend), 1457 (aromatic C═C stretch), 1424 (C−N stretch). ESI$^+$-HRMS: m/z $_{calc}$ = 825.2729 for $C_{47}H_{45}N_7ORu$; m/z $_{found}$ = 412.6378 $[M]^{2+}$.

*Bis(1,4,5,8-tetraazaphenantherene)(N-1,10-phenanthrolin-5-ylacetamide)ruthenium(II) Chloride (**4**).* Complex **4** was synthesized according to the same procedure described for **1** but using *cis*-$[Ru(TAP)_2Cl_2]$ (90.8 mg, 169 μmol, 1 equiv) as precursor complex and ligand **7** (44.1 mg, 186 μmol, 1.1 equiv), yielding the product as a red solid (67.5 mg, 87.2 μmol, 52%). Calculated for $C_{34}H_{23}N_{11}Cl_2ORu + 5.2H_2O + 0.2NaCl$: C, 46.46; H, 3.83; N, 17.53; Cl, 8.87. Found: C, 46.27; H, 3.17; N, 16.89; Cl, 8.66. mp 162−164 °C (decomp.). δ_H (400 MHz, DMSO-d_6): 10.71 (1H, s, NH), 9.06 (5H, m, H_4^{L7} and H^{TAP}), 8.80 (1H, d, H_7^{L7}, ^3J = 8.2 Hz), 8.66 (5H, s, H_6^{L7}, H_9^{TAP} and H_{10}^{TAP}), 8.51 (1H, d, H^{TAP}, ^3J = 2.8 Hz)), 8.48 (1H, d, H^{TAP}, ^3J = 2.8 Hz), 8.30 (1H, d, H_2^{L7}, ^3J = 5.3 Hz), 8.24 (2H, m, H^{TAP}), 8.17 (1H, d, H_9^{L7}, ^3J = 5.3 Hz), 7.82 (1H, dd, H_3^{L7}, ^3J = 5.3 Hz, ^3J = 8.5 Hz), 7.73 (1H, dd, H_8^{L7}, ^3J = 5.3 Hz, ^3J = 8.2 Hz), 2.32 (3H, s, CH_3). δ_C (101 MHz, DMSO-d_6): 169.82 (C═O), 153.94, 152.66, 149.65, 149.50, 148.67, 148.62, 146.82 (q), 144.52 (q), 144.51 (q), 144.48 (q), 144.06 (q), 141.98 (q), 141.93 (q), 141.91 (q), 137.36, 133.92, 132.41, 132.28, 130.34 (q), 126.45 (q), 126.34, 125.64, 119.01, 23.80 (CH_3). ν_{max} (ATR)/cm^{-1}: 3220 (amide N−H stretch), 3052 (aromatic C−H stretch), 2979 (alkane C−H stretch), 1681 (C═O stretch), 1528 (amide N−H bend), 1485 (aromatic C═C stretch), 1383 (C−N stretch). MALDI$^+$-HRMS: m/z $_{calc}$ = 703.1131 for $C_{34}H_{23}N_{11}ORu$; m/z $_{found}$ = 703.1135 $[M]^+$.

*Bis(1,4,5,8-tetraazaphenantherene)(N-1,10-phenanthrolin-5-ylundecanamide)ruthenium(II) Chloride (**5**).* Complex **5** was synthesized according to the same procedure described for **1** but using *cis*-$[Ru(TAP)_2Cl_2]$ (101 mg, 192 μmol, 1 equiv) as precursor complex and ligand **8** (82.5 mg, 227 μmol, 1.2 equiv), yielding the product as a red solid (73.0 mg, 81.1 μmol, 43%). Calculated for $C_{43}H_{41}N_{11}Cl_2ORu + 4.6H_2O + 0.1NaCl$: C, 52.24; H, 5.12; N, 15.59; Cl, 7.53. Found: C, 51.89; H, 4.45; N, 15.34; Cl, 6.93. mp 150−151 °C (decomp.). δ_H (400 MHz, CD_3CN): 11.67 (1H, s, NH), 9.71 (1H, d, H_4^{L8}, ^3J = 8.5 Hz), 8.94 (4H, m, H^{TAP}), 8.69 (1H, s, H_6^{L8}), 8.58 (5H, s, H_7^{L8}, H_9^{TAP} and H_{10}^{TAP}), 8.29 (1H, d, H^{TAP}, ^3J = 2.7 Hz), 8.27 (1H, d, H^{TAP}, ^3J = 2.7 Hz), 8.20 (1H, d, H^{TAP}, ^3J = 2.7 Hz), 8.16 (1H, d, H^{TAP}, ^3J = 2.7 Hz), 8.14 (1H, d, H_2^{L8}, ^3J = 5.1 Hz), 7.99 (1H, d, H_9^{L8}, ^3J = 5.1 Hz), 7.70 (1H, dd, H_3^{L8}, ^3J = 5.1 Hz, ^3J = 8.5 Hz), 7.60 (1H, dd, H_8^{L8}, ^3J = 5.1 Hz, ^3J = 8.5 Hz), 2.84 (2H, t, $H_{2'}^{L8}$, ^3J = 7.4 Hz), 1.74 (2H, m, $H_{3'}^{L8}$), 1.33 (14H, m, $H_{4'}$−$H_{10'}^{L8}$), 0.86 (3H, t, $H_{11'}^{L8}$, ^3J = 7.0 Hz). δ_C (101 MHz, CD_3CN): 175.04 (C═O), 154.69, 153.19, 150.38, 150.33, 150.30, 150.14, 150.09, 149.84, 149.70, 148.30 (q), 146.38 (q), 146.34 (q), 146.31 (q), 146.28 (q), 145.33 (q), 143.31 (q), 143.28 (q), 143.26 (q), 138.34, 136.99, 136.24 (q), 133.72, 133.55, 132.11 (q), 128.29 (q), 126.90, 125.98, 119.90, 37.31, 32.56, 30.27, 30.17, 30.00, 29.98, 26.55, 23.32, 14.32. ν_{max} (ATR)/cm^{-1}: 3247 (amide N−H stretch), 3048 (aromatic C−H stretch), 2923 and 2852 (alkane C−H stretch), 1671 (C═O stretch), 1535 (amide N−H bend), 1485 (aromatic C═C stretch), 1422 (C−N stretch). ESI$^+$-HRMS: m/z $_{calc}$ = 829.2539 for $C_{43}H_{41}N_{11}ORu$; m/z $_{found}$ = 414.6258 $[M]^{2+}$.

■ ASSOCIATED CONTENT

Supporting Information

The Supporting Information is available free of charge at https://pubs.acs.org/doi/10.1021/acsabm.1c00284.

Figures of NMR, MS, and IR spectra and ground and excited-state changes, and cellular imaging, etc.; tables for binding constants, CD, and excited-state lifetimes (PDF)

Special Issue Paper

This paper missed the Biospecies Sensors Forum special issue.

■ AUTHOR INFORMATION

Corresponding Authors

Sandra Estalayo-Adrián − *School of Chemistry and Trinity Biomedical Sciences Institute (TBSI) and Advanced Materials and BioEngineering Research (AMBER) Centre, Trinity College Dublin, The University of Dublin, Dublin 2, Ireland*; Email: estalays@tcd.ie

Thorfinnur Gunnlaugsson − *School of Chemistry and Trinity Biomedical Sciences Institute (TBSI) and Advanced Materials and BioEngineering Research (AMBER) Centre, Trinity College Dublin, The University of Dublin, Dublin 2, Ireland*; orcid.org/0000-0003-4814-6853; Email: gunnlaut@tcd.ie

Authors

Salvador Blasco − *School of Chemistry and Trinity Biomedical Sciences Institute (TBSI), Trinity College Dublin, The University of Dublin, Dublin 2, Ireland*

Sandra A. Bright − *School of Biochemistry and Immunology, Trinity Biomedical Sciences Institute (TBSI), Trinity College Dublin, The University of Dublin, Dublin 2, Ireland*

Gavin J. McManus − *School of Biochemistry and Immunology, Trinity Biomedical Sciences Institute (TBSI), Trinity College Dublin, The University of Dublin, Dublin 2, Ireland*

Guillermo Orellana − *Department of Organic Chemistry, Faculty of Chemistry, Universidad Complutense de Madrid, E-28040 Madrid, Spain*; orcid.org/0000-0002-4572-6564

D. Clive Williams − *School of Biochemistry and Immunology, Trinity Biomedical Sciences Institute (TBSI), Trinity College Dublin, The University of Dublin, Dublin 2, Ireland*

https://doi.org/10.1021/acsabm.1c00284
ACS Appl. Bio Mater. XXXX, XXX, XXX−XXX

John M. Kelly − *School of Chemistry and Trinity Biomedical Sciences Institute (TBSI), Trinity College Dublin, The University of Dublin, Dublin 2, Ireland;* orcid.org/0000-0002-3706-1777

Complete contact information is available at: https://pubs.acs.org/10.1021/acsabm.1c00284

Notes

The authors declare no competing financial interest.

■ ACKNOWLEDGMENTS

We thank Science Foundation Ireland (SFI PI Awards 10/45 IN.1/B2999 and 13/IA/1865), Marie Skłodowska-Curie actions (MSCA, to S.B.), and Trinity College Dublin (TCD) for financial support. We also thank Drs. Feeney, Hessman, O'Brien, and Ruether for the help with MS and NMR studies.

■ REFERENCES

(1) Juris, A.; Balzani, V.; Barigelletti, F.; Campagna, S.; Belser, P.; von Zelewsky, A. Ru(II) polypyridine complexes: photophysics, photochemistry, eletrochemistry, and chemiluminescence. *Coord. Chem. Rev.* **1988**, *84*, 85−277.

(2) Balzani, V.; Juris, A.; Venturi, M.; Campagna, S.; Serroni, S. Luminescent and Redox-Active Polynuclear Transition Metal Complexes. *Chem. Rev.* **1996**, *96*, 759−834.

(3) Vos, J. G.; Kelly, J. M. Ruthenium polypyridyl chemistry; from basic research to applications and back again. *Dalton Trans.* **2006**, 4869−4883.

(4) Gill, M. R.; Thomas, J. A. Ruthenium(ii) polypyridyl complexes and DNA—from structural probes to cellular imaging and therapeutics. *Chem. Soc. Rev.* **2012**, *41*, 3179−3192.

(5) Mari, C.; Pierroz, V.; Leonidova, A.; Ferrari, S.; Gasser, G. Towards Selective Light-Activated RuII-Based Prodrug Candidates. *Eur. J. Inorg. Chem.* **2015**, *2015*, 3879−3891.

(6) Knoll, J. D.; Turro, C. Control and utilization of ruthenium and rhodium metal complex excited states for photoactivated cancer therapy. *Coord. Chem. Rev.* **2015**, *282*−*283*, 110−126.

(7) Poynton, F. E.; Bright, S. A.; Blasco, S.; Williams, D. C.; Kelly, J. M.; Gunnlaugsson, T. The development of ruthenium(ii) polypyridyl complexes and conjugates for in vitro cellular and in vivo applications. *Chem. Soc. Rev.* **2017**, *46*, 7706−7756.

(8) White, J. K.; Schmehl, R. H.; Turro, C. An overview of photosubstitution reactions of Ru(II) imine complexes and their application in photobiology and photodynamic therapy. *Inorg. Chim. Acta* **2017**, *454*, 7−20.

(9) Thota, S.; Rodrigues, D. A.; Crans, D. C.; Barreiro, E. J. Ru(II) Compounds: Next-Generation Anticancer Metallotherapeutics? *J. Med. Chem.* **2018**, *61*, 5805−5821.

(10) Monro, S.; Colón, K. L.; Yin, H.; Roque, J.; Konda, P.; Gujar, S.; Thummel, R. P.; Lilge, L.; Cameron, C. G.; McFarland, S. A. Transition Metal Complexes and Photodynamic Therapy from a Tumor-Centered Approach: Challenges, Opportunities, and Highlights from the Development of TLD1433. *Chem. Rev.* **2019**, *119*, 797−828.

(11) Shum, J.; Leung, P. K.-K.; Lo, K. K.-W. Luminescent Ruthenium(II) Polypyridine Complexes for a Wide Variety of Biomolecular and Cellular Applications. *Inorg. Chem.* **2019**, *58*, 2231−2247.

(12) Elmes, R. B. P.; Orange, K. N.; Cloonan, S. M.; Williams, D. C.; Gunnlaugsson, T. Luminescent Ruthenium(II) Polypyridyl Functionalized Gold Nanoparticles; Their DNA Binding Abilities and Application As Cellular Imaging Agents. *J. Am. Chem. Soc.* **2011**, *133*, 15862−15865.

(13) Rogers, N. J.; Claire, S.; Harris, R. M.; Farabi, S.; Zikeli, G.; Styles, I. B.; Hodges, N. J.; Pikramenou, Z. High coating of Ru(ii) complexes on gold nanoparticles for single particle luminescence imaging in cells. *Chem. Commun.* **2014**, *50*, 617−619.

(14) Zhang, P.; Wang, J.; Huang, H.; Yu, B.; Qiu, K.; Huang, J.; Wang, S.; Jiang, L.; Gasser, G.; Ji, L.; Chao, H. Unexpected high photothemal conversion efficiency of gold nanospheres upon grafting with two-photon luminescent ruthenium(II) complexes: A way towards cancer therapy? *Biomaterials* **2015**, *63*, 102−114.

(15) Martínez-Calvo, M.; Orange, K. N.; Elmes, R. B. P.; la Cour Poulsen, B.; Williams, D. C.; Gunnlaugsson, T. Ru(ii)-polypyridyl surface functionalised gold nanoparticles as DNA targeting supramolecular structures and luminescent cellular imaging agents. *Nanoscale* **2016**, *8*, 563−574.

(16) Wumaier, M.; Yao, T.-M.; Hu, X.-C.; Hu, Z.-A.; Shi, S. Luminescent Ru(ii)-thiol modified silver nanoparticles for lysosome targeted theranostics. *Dalton Trans.* **2019**, *48*, 10393−10397.

(17) Estalayo-Adrián, S.; McManus, G. J.; Dalton, H. L.; Savyasachi, A. J.; Kelly, J. M.; Gunnlaugsson, T. Functionalisation of gold nanoparticles with ruthenium(ii) polypyridyl complexes for their application in cellular imaging. *Dalton Trans.* **2020**, *49*, 14158−14168.

(18) Puckett, C. A.; Barton, J. K. Fluorescein Redirects a Ruthenium−Octaarginine Conjugate to the Nucleus. *J. Am. Chem. Soc.* **2009**, *131*, 8738−8739.

(19) Puckett, C. A.; Barton, J. K. Targeting a ruthenium complex to the nucleus with short peptides. *Bioorg. Med. Chem.* **2010**, *18*, 3564−3569.

(20) Cosgrave, L.; Devocelle, M.; Forster, R. J.; Keyes, T. E. Multimodal cell imaging by ruthenium polypyridyl labelled cell penetrating peptides. *Chem. Commun.* **2010**, *46*, 103−105.

(21) Blackmore, L.; Moriarty, R.; Dolan, C.; Adamson, K.; Forster, R. J.; Devocelle, M.; Keyes, T. E. Peptide directed transmembrane transport and nuclear localization of Ru(ii) polypyridyl complexes in mammalian cells. *Chem. Commun.* **2013**, *49*, 2658−2660.

(22) Joshi, T.; Pierroz, V.; Ferrari, S.; Gasser, G. Bis-(dipyridophenazine)(2-(2′-pyridyl)pyrimidine-4-carboxylic acid)-ruthenium(II) Hexafluorophosphate: A Lesson in Stubbornness. *ChemMedChem* **2014**, *9*, 1419−1427.

(23) Marcélis, L.; Kajouj, S.; Ghesquière, J.; Fettweis, G.; Coupienne, I.; Lartia, R.; Surin, M.; Defrancq, E.; Piette, J.; Moucheron, C.; Kirsch-De Mesmaeker, A. Highly DNA-Photoreactive Ruthenium 1,4,5,8-Tetraazaphenanthrene Complex Conjugated to the TAT Peptide: Efficient Vectorization inside HeLa Cells without Phototoxicity − The Importance of Cellular Distribution. *Eur. J. Inorg. Chem.* **2016**, *2016*, 2902−2911.

(24) Huang, H.; Yu, B.; Zhang, P.; Huang, J.; Chen, Y.; Gasser, G.; Ji, L.; Chao, H. Highly Charged Ruthenium(II) Polypyridyl Complexes as Lysosome-Localized Photosensitizers for Two-Photon Photodynamic Therapy. *Angew. Chem., Int. Ed.* **2015**, *54*, 14049−14052.

(25) Burke, C. S.; Byrne, A.; Keyes, T. E. Highly Selective Mitochondrial Targeting by a Ruthenium(II) Peptide Conjugate: Imaging and Photoinduced Damage of Mitochondrial DNA. *Angew. Chem., Int. Ed.* **2018**, *57*, 12420−12424.

(26) Gottschaldt, M.; Schubert, U. S.; Rau, S.; Yano, S.; Vos, J. G.; Kroll, T.; Clement, J.; Hilger, I. Sugar-Selective Enrichment of a D-Glucose-Substituted Ruthenium Bipyridyl Complex Inside HepG2 Cancer Cells. *ChemBioChem* **2010**, *11*, 649−652.

(27) Wenzel, M.; de Almeida, A.; Bigaeva, E.; Kavanagh, P.; Picquet, M.; Le Gendre, P.; Bodio, E.; Casini, A. New Luminescent Polynuclear Metal Complexes with Anticancer Properties: Toward Structure−Activity Relationships. *Inorg. Chem.* **2016**, *55*, 2544−2557.

(28) Lameijer, L. N.; Hopkins, S. L.; Brevé, T. G.; Askes, S. H. C.; Bonnet, S. d- Versus l-Glucose Conjugation: Mitochondrial Targeting of a Light-Activated Dual-Mode-of-Action Ruthenium-Based Anticancer Prodrug. *Chem. - Eur. J.* **2016**, *22*, 18484−18491.

(29) Lo, K. K.-W.; Lee, T. K.-M.; Lau, J. S.-Y.; Poon, W.-L.; Cheng, S.-H. Luminescent Biological Probes Derived from Ruthenium(II) Estradiol Polypyridine Complexes. *Inorg. Chem.* **2008**, *47*, 200−208.

(30) Dosio, F.; Stella, B.; Ferrero, A.; Garino, C.; Zonari, D.; Arpicco, S.; Cattel, L.; Giordano, S.; Gobetto, R. Ruthenium polypyridyl squalene derivative: A novel self-assembling lipophilic probe for cellular imaging. *Int. J. Pharm.* **2013**, *440*, 221−228.

(31) Siewert, B.; van Rixel, V. H. S.; van Rooden, E. J.; Hopkins, S. L.; Moester, M. J. B.; Ariese, F.; Siegler, M. A.; Bonnet, S. Chemical Swarming: Depending on Concentration, an Amphiphilic Ruthenium Polypyridyl Complex Induces Cell Death via Two Different Mechanisms. *Chem. - Eur. J.* **2016**, *22*, 10960−10968.
(32) Schatzschneider, U.; Niesel, J.; Ott, I.; Gust, R.; Alborzinia, H.; Wölfl, S. Cellular Uptake, Cytotoxicity, and Metabolic Profiling of Human Cancer Cells Treated with Ruthenium(II) Polypyridyl Complexes $[Ru(bpy)_2(N{-}N)]Cl_2$ with N−N═bpy, phen, dpq, dppz, and dppn. *ChemMedChem* **2008**, *3*, 1104−1109.
(33) Cloonan, S. M.; Elmes, R. B. P.; Erby, M.; Bright, S. A.; Poynton, F. E.; Nolan, D. E.; Quinn, S. J.; Gunnlaugsson, T.; Williams, D. C. Detailed Biological Profiling of a Photoactivated and Apoptosis Inducing pdppz Ruthenium(II) Polypyridyl Complex in Cancer Cells. *J. Med. Chem.* **2015**, *58*, 4494−4505.
(34) Poulsen, B. C.; Estalayo-Adrián, S.; Blasco, S.; Bright, S. A.; Kelly, J. M.; Williams, D. C.; Gunnlaugsson, T. Luminescent ruthenium polypyridyl complexes with extended 'dppz' like ligands as DNA targeting binders and cellular agents. *Dalton Trans.* **2016**, *45*, 18208−18220.
(35) Puckett, C. A.; Barton, J. K. Methods to Explore Cellular Uptake of Ruthenium Complexes. *J. Am. Chem. Soc.* **2007**, *129*, 46−47.
(36) Svensson, F. R.; Matson, M.; Li, M.; Lincoln, P. Lipophilic ruthenium complexes with tuned cell membrane affinity and photoactivated uptake. *Biophys. Chem.* **2010**, *149*, 102−106.
(37) Johnson, I. D., Probes for Lipids and Membranes. In *Molecular Probes Handbook: A Guide to Fluorescent Probes and Labeling Technologies*, 11th ed.; Thermo Fisher Scientific, 2010; Chapter 13.
(38) Li, L.; Szmacinski, H.; Lakowicz, J. R. Synthesis and Luminescence Spectral Characterization of Long-Lifetime Lipid Metal−Ligand Probes. *Anal. Biochem.* **1997**, *244*, 80−85.
(39) Svensson, F. R.; Li, M.; Nordén, B.; Lincoln, P. Luminescent Dipyridophenazine-Ruthenium Probes for Liposome Membranes. *J. Phys. Chem. B* **2008**, *112*, 10969−10975.
(40) Mechler, A.; Stringer, B. D.; Mubin, M. S. H.; Doeven, E. H.; Phillips, N. W.; Rudd-Schmidt, J.; Hogan, C. F. Labeling phospholipid membranes with lipid mimetic luminescent metal complexes. *Biochim. Biophys. Acta, Biomembr.* **2014**, *1838*, 2939−2946.
(41) KaŠČáková, S.; Giuliani, A.; Lacerda, S.; Pallier, A.; Mercère, P.; Tóth, É.; Réfrégiers, M. X-ray-induced radiophotodynamic therapy (RPDT) using lanthanide micelles: Beyond depth limitations. *Nano Res.* **2015**, *8*, 2373−2379.
(42) Verwilst, P.; Park, S.; Yoon, B.; Kim, J. S. Recent advances in Gd-chelate based bimodal optical/MRI contrast agents. *Chem. Soc. Rev.* **2015**, *44*, 1791−1806.
(43) Arroyo, I. Z.; Gomez, C.; Alarcon, H.; Jimenez, A.; Pardo, A.; Montaño, G.; Armijos, R. X.; Noveron, J. C. Alkyl Length Effects on the DNA Transport Properties of Cu(II) and Zn(II) Metallovesicles: An In Vitro and In Vivo Study. *J. Drug Delivery* **2018**, *2018*, 2851579.
(44) Griffiths, P. C.; Fallis, I. A.; Chuenpratoom, T.; Watanesk, R. Metallosurfactants: Interfaces and micelles. *Adv. Colloid Interface Sci.* **2006**, *122*, 107−117.
(45) Komatsu, H.; Yoshihara, K.; Yamada, H.; Kimura, Y.; Son, A.; Nishimoto, S.-i.; Tanabe, K. Ruthenium Complexes with Hydrophobic Ligands That Are Key Factors for the Optical Imaging of Physiological Hypoxia. *Chem. - Eur. J.* **2013**, *19*, 1971−1977.
(46) Nagaraj, K.; Murugan, K. S.; Thangamuniyandi, P.; Sakthinathan, S. Nucleic acid binding study of surfactant copper(ii) complex containing dipyrido[3,2-a:2′-3′-c]phenazine ligand as an intercalator: in vitro antitumor activity of complex in human liver carcinoma (HepG2) cancer cells. *RSC Adv.* **2014**, *4*, 56084−56094.
(47) Lebrón, J. A.; Ostos, F. J.; Moyá, M. L.; López-López, M.; Carrasco, C. J.; López-Cornejo, P. Cooperative interaction between metallosurfactants, derived from the [Ru(2,2′-bpy)3]2+ complex, and DNA. *Colloids Surf., B* **2015**, *135*, 817−824.
(48) Estalayo-Adrián, S.; Blasco, S.; Bright, S. A.; McManus, G. J.; Orellana, G.; Williams, D. C.; Kelly, J. M.; Gunnlaugsson, T. Water-soluble amphiphilic ruthenium(ii) polypyridyl complexes as potential light-activated therapeutic agents. *Chem. Commun.* **2020**, *56*, 9332−9335.
(49) Del Guerzo, A.; Kirsch-De Mesmaeker, A.; Demeunynck, M.; Lhomme, J. Characterisation of bifunctional ruthenium(II) complexes, potential DNA photo-probes. Presence of folded and unfolded conformers. *J. Chem. Soc., Dalton Trans.* **2000**, 1173−1180.
(50) Herman, L.; Elias, B.; Pierard, F.; Moucheron, C.; Kirsch-De Mesmaeker, A. Effects of Protonation on the Spectroscopic Properties of Tetrapyridoacridine (TPAC) Mono- and Dinuclear Ru(II) Complexes in Their Ground and 3MLCT Excited States. *J. Phys. Chem. A* **2007**, *111*, 9756−9763.
(51) Ortmans, I.; Elias, B.; Kelly, J. M.; Moucheron, C.; Kirsch-DeMesmaeker, A. [Ru(TAP)2(dppz)]2+: a DNA intercalating complex, which luminesces strongly in water and undergoes photo-induced proton-coupled electron transfer with guanosine-5′-monophosphate. *Dalton Trans.* **2004**, 668−676.
(52) Lecomte, J.-P.; Kirsch-De Mesmaeker, A.; Kelly, J. M.; Tossi, A. B.; Görner, H. Photo-induced electron transfer from nucleotides to ruthenium-tris-1,4,5,8-tetraazaphenanthrene: model for photosensitized DNA oxidation. *Photochem. Photobiol.* **1992**, *55*, 681−689.
(53) Lecomte, J.-P.; Kirsch-De Mesmaeker, A.; Feeney, M. M.; Kelly, J. M. Ruthenium(II) Complexes with 1,4,5,8,9,12-Hexaazatriphenylene and 1,4,5,8-Tetraazaphenanthrene Ligands: Key Role Played by the Photoelectron Transfer in DNA Cleavage and Adduct Formation. *Inorg. Chem.* **1995**, *34*, 6481−6491.
(54) Kajouj, S.; Marcélis, L.; Lemaur, V.; Beljonne, D.; Moucheron, C. Photochemistry of ruthenium(ii) complexes based on 1,4,5,8-tetraazaphenanthrene and 2,2′-bipyrazine: a comprehensive experimental and theoretical study. *Dalton Trans.* **2017**, *46*, 6623−6633.
(55) García-Fresnadillo, D.; Georgiadou, Y.; Orellana, G.; Braun, A. M.; Oliveros, E. Singlet-Oxygen (1Δg) Production by Ruthenium(II) complexes containing polyazaheterocyclic ligands in methanol and in water. *Helv. Chim. Acta* **1996**, *79*, 1222−1238.
(56) Carraway, E. R.; Demas, J. N.; DeGraff, B. A. Luminescence quenching mechanism for microheterogeneous systems. *Anal. Chem.* **1991**, *63*, 332−336.
(57) García-Fresnadillo, D.; Orellana, G. Interaction of Sulfonated Ruthenium(II) Polypyridine Complexes with Surfactants Probed by Luminescence Spectroscopy. *Helv. Chim. Acta* **2001**, *84*, 2708−2730.
(58) Suzuki, K.; Kobayashi, A.; Kaneko, S.; Takehira, K.; Yoshihara, T.; Ishida, H.; Shiina, Y.; Oishi, S.; Tobita, S. Reevaluation of absolute luminescence quantum yields of standard solutions using a spectrometer with an integrating sphere and a back-thinned CCD detector. *Phys. Chem. Chem. Phys.* **2009**, *11*, 9850−9860.
(59) Hergueta-Bravo, A.; Jiménez-Hernández, M. E.; Montero, F.; Oliveros, E.; Orellana, G. Singlet Oxygen-Mediated DNA Photocleavage with Ru(II) Polypyridyl Complexes. *J. Phys. Chem. B* **2002**, *106*, 4010−4017.
(60) Elias, B.; Kirsch-De Mesmaeker, A. Photo-reduction of polyazaaromatic Ru(II) complexes by biomolecules and possible applications. *Coord. Chem. Rev.* **2006**, *250*, 1627−1641.
(61) Entradas, T.; Waldron, S.; Volk, M. The detection sensitivity of commonly used singlet oxygen probes in aqueous environments. *J. Photochem. Photobiol., B* **2020**, *204*, 111787.
(62) In order to exclude any degradation of ABDA upon irradiation, the emission spectrum of ABDA in the absence of the Ru(II) complexes was also recorded at different irradiation times. No change in the emission intensity of ABDA at 405 nm was observed with the irradiation time, further demonstrating that the changes observed in the presence of 1, 2, 4, and 5 are due to the 1O2 production by the complexes.
(63) Marcélis, L.; Ghesquière, J.; Garnir, K.; Kirsch-De Mesmaeker, A.; Moucheron, C. Photo-oxidizing RuII complexes and light: Targeting biomolecules via photoadditions. *Coord. Chem. Rev.* **2012**, *256*, 1569−1582.
(64) Estalayo-Adrián, S.; Garnir, K.; Moucheron, C. Perspectives of ruthenium(ii) polyazaaromatic photo-oxidizing complexes photoreactive towards tryptophan-containing peptides and derivatives. *Chem. Commun.* **2018**, *54*, 322−337.

https://doi.org/10.1021/acsabm.1c00284
ACS Appl. Bio Mater. XXXX, XXX, XXX−XXX

(65) Kotani, H.; Ohkubo, K.; Fukuzumi, S. Photocatalytic Oxygenation of Anthracenes and Olefins with Dioxygen via Selective Radical Coupling Using 9-Mesityl-10-methylacridinium Ion as an Effective Electron-Transfer Photocatalyst. *J. Am. Chem. Soc.* **2004**, *126*, 15999−16006.
(66) The oxidation potential of ABDA has not been previously determined and as such the value reported for 9,10-dimethylanthracene was used instead, assuming that the malonic acid moiety in ABDA did not have a strong effect in the oxidation potential of the anthracene derivative.
(67) Wessels, J. M.; Foote, C. S.; Ford, W. E.; Rodgers, M. A. J. Photooxidation of Tryptophan: O2(1Δg) versus Electron-Transfer Pathway. *Photochem. Photobiol.* **1997**, *65*, 96−102.
(68) Carter, M. T.; Rodriguez, M.; Bard, A. J. Voltammetric studies of the interaction of metal chelates with DNA. 2. Tris-chelated complexes of cobalt(III) and iron(II) with 1,10-phenanthroline and 2,2′-bipyridine. *J. Am. Chem. Soc.* **1989**, *111*, 8901−8911.
(69) Poulsen, B. C.; Estalayo-Adrián, S.; Blasco, S.; Bright, S. A.; Kelly, J. M.; Williams, D. C.; Gunnlaugsson, T. Luminescent ruthenium polypyridyl complexes with extended 'dppz' like ligands as DNA targeting binders and cellular agents. *Dalton Trans.* **2016**, *45*, 18208−18220.
(70) Haworth, I. S.; Elcock, A. H.; Rodger, A.; Richards, W. G. A Binding Mode of Δ-[tris(1,10-phenanthroline)ruthenium(II)]2+ Exhibiting Preference for Purine-3′,5′-Pyrimidine Sites of DNA. *J. Biomol. Struct. Dyn.* **1991**, *9*, 553−569.
(71) Eriksson, M.; Leijon, M.; Hiort, C.; Norden, B.; Graeslund, A. Binding of DELTA- and LAMBDA-[Ru(phen)3]2+ to [d-(CGCGATCGCG)]2 Studied by NMR. *Biochemistry* **1994**, *33*, 5031−5040.
(72) Husale, S.; Grange, W.; Karle, M.; Bürgi, S.; Hegner, M. Interaction of cationic surfactants with DNA: a single-molecule study. *Nucleic Acids Res.* **2008**, *36*, 1443−1449.
(73) Guo, L.; Zhang, Z.; Qiao, H.; Liu, M.; Shen, M.; Yuan, T.; Chen, J.; Dionysiou, D. D. Spectroscopic study on interaction between three cationic surfactants with different alkyl chain lengths and DNA. *Spectrochim. Acta, Part A* **2015**, *151*, 237−246.
(74) Guo, Q.; Zhang, Z.; Song, Y.; Liu, S.; Gao, W.; Qiao, H.; Guo, L.; Wang, J. Investigation on interaction of DNA and several cationic surfactants with different head groups by spectroscopy, gel electrophoresis and viscosity technologies. *Chemosphere* **2017**, *168*, 599−605.
(75) Nagaraj, K.; Velmurugan, G.; Sakthinathan, S.; Venuvanalingam, P.; Arunachalam, S. Influence of self-assembly on intercalative DNA binding interaction of double-chain surfactant Co(iii) complexes containing imidazo[4,5-f][1,10]phenanthroline and dipyrido[3,2-d:2′-3′-f]quinoxaline ligands: experimental and theoretical study. *Dalton Trans.* **2014**, *43*, 18074−18086.
(76) Nehru, S.; Veeralakshmi, S.; Kalaiselvam, S.; Subin David, S. P.; Sandhya, J.; Arunachalam, S. DNA binding, antibacterial, hemolytic and anticancer studies of some fluorescent emissive surfactant-ruthenium(II) complexes. *J. Biomol. Struct. Dyn.* **2021**, *39*, 2242−2256.
(77) Kelly, J. M.; Tossi, A. B.; McConnell, D. J.; OhUigin, C. A study of the interactions of some polypyridylruthenium (II) complexes with DNA using fluorescence spectroscopy, topoisomerisation and thermal denaturation. *Nucleic Acids Res.* **1985**, *13*, 6017−6034.
(78) Comment: It must be noted that since the complexes discussed here do not contain ionizable groups, they are not expected to be protonated/deprotonated at physiological pH, and as such log *P* values were calculated instead of the logarithm of their distribution coefficient (log *D*).
(79) Gorle, A. K.; Feterl, M.; Warner, J. M.; Wallace, L.; Keene, F. R.; Collins, J. G. Tri- and tetra-nuclear polypyridyl ruthenium(ii) complexes as antimicrobial agents. *Dalton Trans.* **2014**, *43*, 16713−16725.
(80) Gill, M. R.; Garcia-Lara, J.; Foster, S. J.; Smythe, C.; Battaglia, G.; Thomas, J. A. A ruthenium(II) polypyridyl complex for direct imaging of DNA structure in living cells. *Nat. Chem.* **2009**, *1*, 662−667.
(81) Dobrucki, J. W. Interaction of oxygen-sensitive luminescent probes Ru(phen)32+ and Ru(bipy)32+ with animal and plant cells in vitro: Mechanism of phototoxicity and conditions for non-invasive oxygen measurements. *J. Photochem. Photobiol., B* **2001**, *65*, 136−144.
(82) Svensson, F. R.; Abrahamsson, M.; Strömberg, N.; Ewing, A. G.; Lincoln, P. Ruthenium(II) Complex Enantiomers as Cellular Probes for Diastereomeric Interactions in Confocal and Fluorescence Lifetime Imaging Microscopy. *J. Phys. Chem. Lett.* **2011**, *2*, 397−401.
(83) Huang, H.; Yu, B.; Zhang, P.; Huang, J.; Chen, Y.; Gasser, G.; Ji, L.; Chao, H. Highly Charged Ruthenium(II) Polypyridyl Complexes as Lysosome-Localized Photosensitizers for Two-Photon Photodynamic Therapy. *Angew. Chem., Int. Ed.* **2015**, *54*, 14049−14052.
(84) Martinez, L. A.; Martínez, C. G.; Klopotek, B. B.; Lang, J.; Neuner, A.; Braun, A. M.; Oliveros, E. Nonradiative and radiative deactivation of singlet molecular oxygen (O2(a1Δg)) in micellar media and microemulsions. *J. Photochem. Photobiol., B* **2000**, *58*, 94−107.
(85) González-Béjar, M.; Liras, M.; Francés-Soriano, L.; Voliani, V.; Herranz-Pérez, V.; Duran-Moreno, M.; Garcia-Verdugo, J. M.; Alarcon, E. I.; Scaiano, J. C.; Pérez-Prieto, J. NIR excitation of upconversion nanohybrids containing a surface grafted Bodipy induces oxygen-mediated cancer cell death. *J. Mater. Chem. B* **2014**, *2*, 4554−4563.
(86) Nasielski-Hinkens, R.; Benedek-Vamos, M.; Hautain, Y.; Nasielski, J. ^{1}H-NMR spectra of pyrazino [2,3-f] quinoxalines and 5,6-diaminoquinoxalines. *Bull. Soc. Chim. Belg.* **1976**, *85*, 781−786.
(87) Lecomte, J. P.; Kirsch-De Mesmaeker, A.; Demeunynck, M.; Lhomme, J. Synthesis and characterisation of a new DNA-binding bifunctional ruthenium(II) complex. *J. Chem. Soc., Faraday Trans.* **1993**, *89*, 3261−3269.
(88) Doi, T.; Nagamiya, H.; Kokubo, M.; Hirabayashi, K.; Takahashi, T. Synthesis of a tetrabenzyl-substituted 10-membered cyclic diamide. *Tetrahedron* **2002**, *58*, 2957−2963.

https://doi.org/10.1021/acsabm.1c00284
ACS Appl. Bio Mater. XXXX, XXX, XXX−XXX